Report No. CDOT-DTD-UCB-95-16

A CASE STUDY OF CONCRETE DECK BEHAVIOR IN A FOUR-SPAN PRESTRESSED GIRDER BRIDGE: FINAL REPORT

by

Li Cao
John H. Allen
P. Benson Shing
University of Colorado

Dave Woodham
Colorado Department of Transportation

September, 1995
Department of Civil, Environmental,
& Architectural Engineering
University of Colorado
Boulder, CO 80309-0428
Research Series No. CU/SR-95/1

Colorado Department of Transportation
4201 E. Arkansas Ave, Denver, CO 80222

Prepared in cooperation with the
U.S. Department of Transportation
Federal Highway Administration

The contents of this report reflect the views of the authors who are responsible for the facts and the accuracy of the data presented herein. The contents do not necessarily reflect the official view of the Colorado Department of Transportation or the Department of Transportation, Federal Highway Administration. This report does not constitute a standard, specification, or regulation.

Technical Report Documentation Page

1. Report No.	2. Government Accession No.	3. Recipient's Catalog No.
CDOT-DTD-UCB-95-16		

4. Title and Subtitle	5. Report Date
A Case Study of Concrete Deck Behavior in a Four-Span Prestressed Girder Bridge: Final Report	January, 1993
	6. Performing Organization Code

7. Author(s)	8. Performing Organization Rpt. No.
Li Cao, John H. Allen, P. Benson Shing	Research Series CU/SR-93/1

9. Performing Organization Name and Address	10. Work Unit No. (TRAIS)
University of Colorado at Boulder Dept. of Civil, Environmental, & Architectural Engineering Boulder, CO 80309-0428	11. Contract or Grant No. DOT92-061

12. Sponsoring Agency Name and Address	13. Type of Rpt. and Period Covered
Colorado Department of Transportation 4201 E. Arkansas Ave. Denver, Colorado 80222	Final, 6/92 to 6/95 14. Sponsoring Agency Code 80.00

15. Supplementary Notes

Prepared in Cooperation with the U.S. Department of Transportation Federal Highway Administration

16. Abstract

A substantial amount of deterioration of bridge decks is caused by corrosion of the top mat of steel. Evidence suggests that the actual tensile stresses at the upper surface of bridge decks are low. This reduces or eliminates the need for top reinforcement except for continuity over supports.

One span of a four-span bridge was constructed without an upper mat of steel. A series of load tests were conducted to induce high strains in the deck. Peak transverse tensile stresses were less than 30% of the concrete cracking strength. This study indicates that conventionally designed bridge decks do not require top steel for sustaining transverse tensile stresses induced by traffic.

Implementation:

This technique will need further study before implementation can proceed.

17. Key Words	18. Distribution Statement
bridge deck, corrosion, reinforcement, strain gages	No Restrictions: This report is available to the public through the National Technical Info. Service, Springfield, VA 22161

19. Security Classif. (report)	20. Security Classif. (page)	21. No. of Pages	22. Price
Unclassified	Unclassified	62	

Abstract

A major cause of the deterioration of bridge decks is the spalling and delamination of deck concrete caused by the corrosion of the top mat of reinforcing bars. Empirical evidence has indicated that the tensile bending stresses developed at the top of a bridge deck subjected to traffic loads are relatively low. As a result, the need for top reinforcing bars for sustaining the negative bending moment induced by traffic loads is questionable. To explore the possibility of eliminating top reinforcing bars and, thereby, reducing the vulnerability to corrosion, the performance of a four-span bridge deck is investigated.

In the bridge studied, one span has an experimental deck, which has no top reinforcement, while the remainder has both top and bottom reinforcement, which conforms to AASHTO Specifications. Two series of load tests were conducted on the bridge. The response of the bridge deck under test trucks was monitored with embedded strain gages. From the results of the first series of load tests, it was found that the peak transverse tensile strains developed at the top of the deck were less than 30% of the cracking strain of the deck concrete. This observation was confirmed by the results of the second series of load tests. Furthermore, there is no significant difference in performance observed from the results of the two series of load tests conducted approximately eighteen months apart. This study indicates that a properly designed bridge deck does not require the top reinforcement for sustaining the negative bending moment induced by traffic loads.

Acknowledgments

The writers gratefully acknowledge the financial support and technical cooperation provided by the Colorado Department of Transportation for this study. However, opinions expressed in this report are those of the writers and do not necessarily represent those of the sponsor.

Contents

List of Figures

List of Tables

Chapter 1

INTRODUCTION

The deterioration of bridges in the United States is a serious problem. As bridges age, repair and replacement needs accrue. It has been estimated that 41% of the nation's 578,000 bridges are either structurally deficient or functionally obsolete (*U.S. Department of Transportation* 1989). An estimated investment of $51 billion is needed to bring all the nation's bridges to an acceptable and safe standard by either rehabilitation or replacement. A substantial portion of this problem is related to the deterioration of concrete decks caused by the corrosion of reinforcing bars. An effective means to prevent such deterioration is to eliminate top reinforcing bars from a deck. This can lead to substantial savings in construction, maintenance, and repair.

In North America, most short and medium span bridges are constructed with slab-on-girder decks, where a reinforced concrete slab is supported by several steel or precast prestressed concrete girders. The current AASHTO slab design provisions (AASHTO 1992) are based upon empirical rules derived from earlier adaptations of the Westergaard Theory (Westergaard 1930, AASHTO 1935, 1957-1961). However, Newmark (Newmark 1949) investigated the behavior of bridge decks and recommended that the slab de-

sign moment should account for girder deflections. Because of girder deflections, the maximum stresses in a bridge deck may vary significantly from those predicted by the design moments according to AASHTO Specifications (AASHTO 1992). Nevertheless, his recommendation has not been adopted in bridge design. As a result, the same design bending moment is used for the top and bottom transverse reinforcing bars of a slab. This necessitates the placement of both an upper and a lower mat of reinforcing bars in a deck. The upper mat contains a top layer of transverse reinforcing bars over a longitudinal layer of bars.

Recently, it has been observed that shrinkage cracks often occur over the upper transverse bars, permitting increased exposure to deleterious substances such as de-icing chemicals. However, longitudinal cracks are not prevalent over the girders. Investigations on the behavior of bridge decks by Beal (Beal 1982) and Fang et al. (Fang 1990) have shown that the negative bending moments in bridge decks and the resulting top tensile stresses are usually very low, much less than the positive bending moments and the resulting bottom tensile stresses. Analysis of their work and other empirical evidence by Allen (Allen 1991) indicate that the tensile strength of deck concrete generally greatly exceeds the top tensile stresses induced by traffic loads, due to the deflection of girders.

With the above observations, one may choose to eliminate most of the upper mat of reinforcing bars in a deck. This can retard deck deterioration, as top reinforcing bars are generally most susceptible to corrosion. To explore this new design concept, an experimental deck was designed and constructed without top reinforcement for an end span of a four-span bridge by the Colorado Department of Transportation. The main objective of this study is to assess the maximum tensile stresses that can be developed in such a deck

as well as its durability in the absence of top reinforcement. The investigation consists of the development of a finite element model for evaluating the response of the deck under truck loads, and the monitoring of the actual response of the bridge deck under test trucks as well as normal traffic loads.

Results of this study were documented in three reports. The results of finite element analysis of the behavior of a four-span bridge deck were documented in a report entitled *"A Case Study of Elastic Concrete Deck Behavior in a Four-Span Prestressed Girder Bridge: Finite Element Analysis" (Report No. CDOT-DTD-CU-93-7).* The results of the first series of load tests conducted on the prototype deck were documented in a report entitled *"A Case Study of Concrete Deck Behavior in a Four-Span Prestressed Girder Bridge: Correlation of Field Tests and Numerical Results" (Report No. CDOT-CU-R-94-8).* In this report, the results of the second series of load tests are presented.

Chapter 2

DESCRIPTION OF BRIDGE DECK AND FIELD TESTS

2.1 Bridge Deck Configuration and Material Properties

The bridge selected for this project is located on Colorado State Route 224 over South Platte River near Commerce City. It is a 420-ft-long and 52-ft-wide bridge. The superstructure consists of four equal continuous spans. The supporting girders are standard precast Colorado Type G-54 girders spaced at approximately eight feet on center. The thickness of the bridge deck is 8.0 inches. The configuration of the four-span bridge and typical girder sections are shown in Fig. 2.1.

In the four-span deck, the west span is the experimental deck which has no top reinforcement. The remaining three spans have both top and bottom reinforcement, conforming to AASHTO Specifications (AASHTO 1992). The deck in the east span is the control deck. Both the experimental and control decks are instrumented with strain gages.

In the control deck, the top and bottom transverse reinforcement consists

of No.5 bars with a 5.5-in center-to-center spacing. The top longitudinal reinforcement consists of No.5 bars with an 18-in center-to-center spacing, and the bottom longitudinal reinforcement consists of No.5 bars with a 9.5-in center-to-center spacing. The clear covers over the top and bottom reinforcing steel are 2.5 and 1.0 inches, respectively.

The experimental deck consists of the entire west span and 38-ft of the adjacent span. The reinforcement of the experimental deck is based on a new design approach, in which the top reinforcement is eliminated. As a result, no top reinforcing steel was placed in the experimental deck, except that there are short transverse bars placed in the cantilever overhangs supporting the railings. Furthermore, in both the experimental and control decks, longitudinal reinforcing bars are placed across the piers with a 9-in center-to-center spacing and a 3-in minimum cover. The reinforcing details of the control and experimental decks are shown in Fig 2.2.

A small amount of fiber was added to the deck concrete to reduce temperature and shrinkage cracks. The specified design strength for the deck concrete was 4,500 psi. The concrete mix consisted of the following ingredients per cubic-yard: 507 lb of cement (Type I/II), 56 lb of fly-ash, 1800 lb of intermediate aggregate (0.75 in), 1240 lb of sand, 1.5 lb of fiber (polypropylene), with a water-cement ratio of 0.47.

With the lab-cured specimens of deck concrete, the average 28-day compressive strength and the modulus of rupture obtained are 5,740 psi and 590 psi, respectively, and the 33-day split-cylinder strength is 350 psi. The average 28-day compressive strength of lab-cured specimens of girder concrete is 8,500 psi.

The bridge was constructed in two phases to facilitate the flow of traffic. The phase-one portion of the deck consists of a 34-ft-wide slab supported

over five girders. It was cast in January, 1993. The phase-two portion of the deck was cast in July, 1993. After the bridge had been opened to traffic for six months, the first series of load tests were conducted on September 11, 1993, with the complete bridge temporarily closed to traffic. Eighteen months later, the same series of load tests were repeated on March 17, 1995 to inspect any changes in the deck behavior. This report documents the results of the second series of load tests.

2.2 Test Truck and Truck Load Positions

As shown in Figs. 2.3 and 2.4, the test trucks used for the first series and the second series of load tests weighed 106 and 104 kips, respectively. The test truck used for the second series of load tests was 1.9% lighter than that of the test truck used for the first series of load tests.

The test truck positions on the bridge deck are the same for the two series of load tests. The test truck was positioned at three different locations along the longitudinal direction of the bridge at the west end, as shown in Fig. 2.5. The first truck position was close to the abutment in the experimental deck, with the resultant of the rear tandem axle loads at approximately 8 feet away from the abutment. The second truck position in the longitudinal direction was near the mid-span of the experimental deck, with the resultant of the rear tandem axle loads at approximately 44 feet away from the abutment. The third truck load position in the longitudinal direction was in the vicinity of the pier in the experimental deck, with the resultant of the rear tandem axle loads at approximately 6 feet away from the pier. The above positions are identified as Load Groups 1, 2, and 3, respectively. As illustrated in Fig. 2.6, the wheels of the test truck were positioned at six to seven different

locations along the transverse direction of the deck for each of the above load groups. In addition to the above three longitudinal positions, the test truck was also placed on the control deck. Load Groups 4 and 5 correspond to the mid-span and abutment positions on the control deck in the east span, which are similar to Load Groups 2 and 1, respectively.

2.3 Instrumentation

The response of the bridge deck under the test trucks was monitored by strain gages embedded at different locations in the deck. These locations are associated with the designated positions of the test trucks discussed above. Five gage lines are selected, as shown in Fig. 2.7. The first three gage lines are located in the experimental deck and the other two in the control deck. In the experimental deck, the first and second gage lines are 6 and 44 feet away from the abutment, respectively. The third gage line is 8 feet away from the pier. Gage Lines 4 and 5 are located in the control deck.

There are seven gage points (A through G) along each of the above gage lines, as shown in Fig. 2.7. Each gage point usually has top and bottom gages, which are oriented in the transverse and longitudinal directions of the deck. The top and bottom gages are about 1 inch away from the top and bottom surfaces of the deck, respectively. The strain gages were welded on 21-in-long No. 4 bars that have anchoring hooks. These bars are embedded in concrete.

2.4 Pre-Test Crack Observation

The cracking patterns of the bridge deck observed before the second series of load tests are illustrated in Figs. 2.8 and 2.9. The dashed lines indicate

cracks observed right before the first series of load tests, while the solid lines indicate the additional cracks observed before the second series of load tests. It was observed that the major change since the first series of load tests is a longitudinal crack extending from the abutment to the pier in the experimental deck, about 8 inches away from the edge of the flange of Girder 4 and right above one of the longitudinal bars. This is a location where the bending moment in the slab about the longitudinal axis is expected to be extremely low. Hence, it is most likely caused by temperature and shrinkage effects.

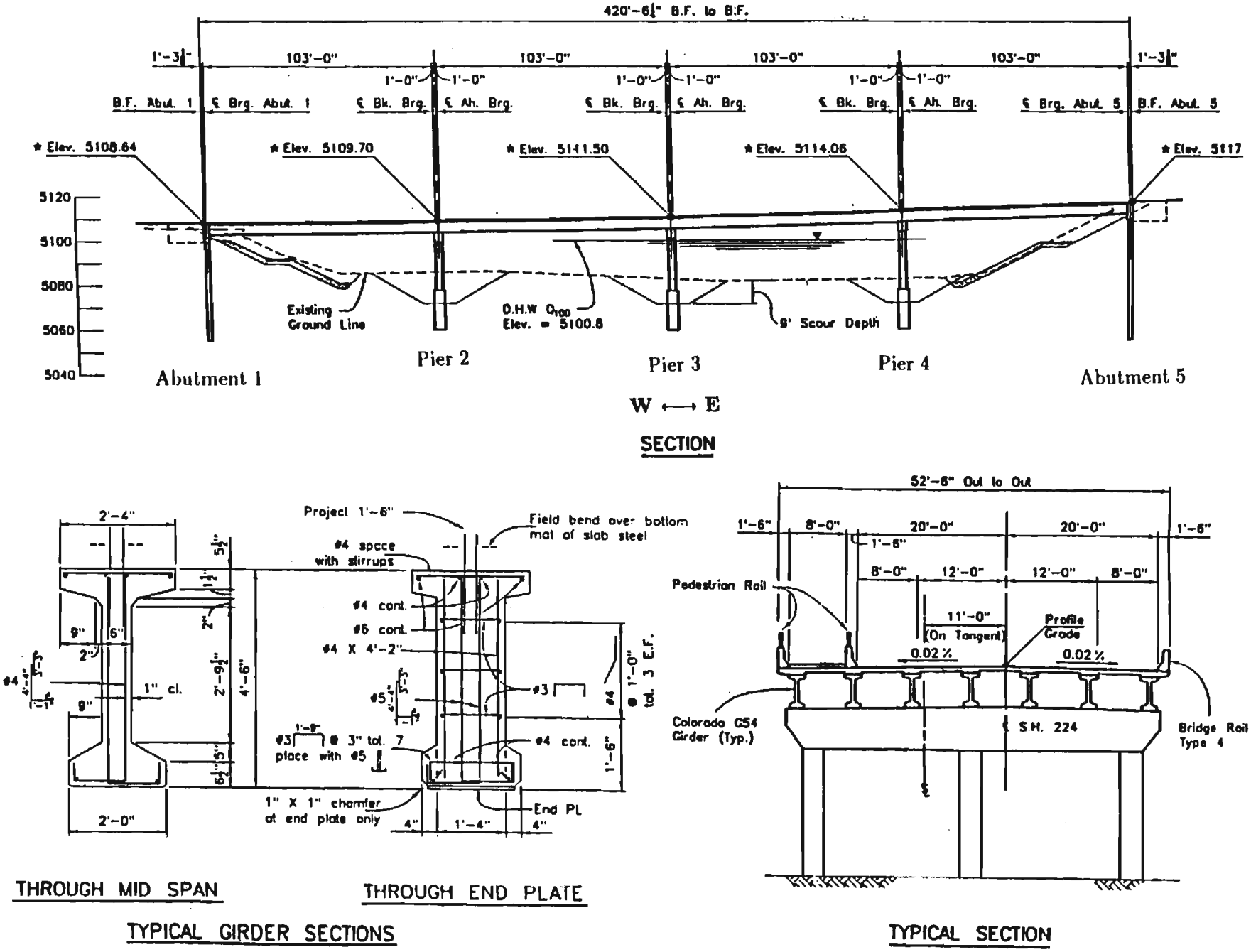

Figure 2.1: Configuration of the Bridge Deck

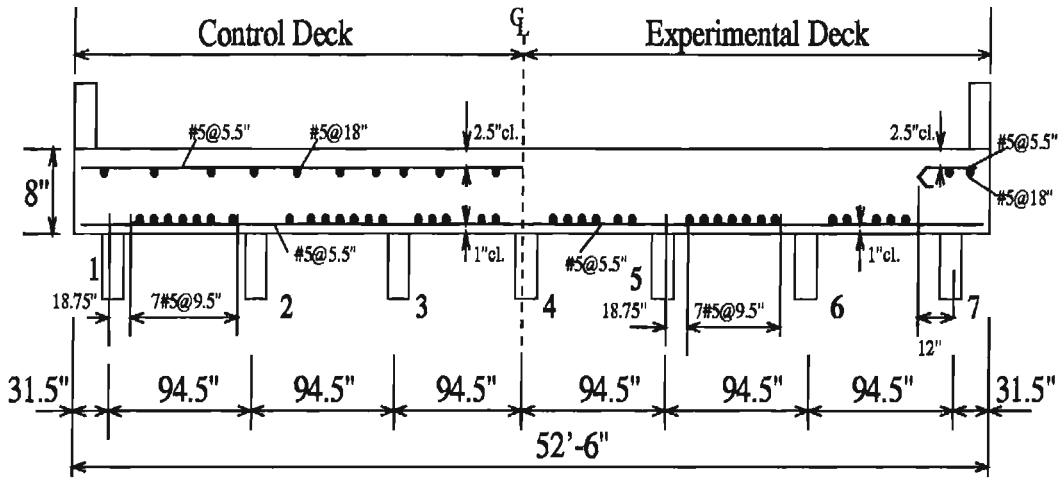

(a) Near Mid-Span

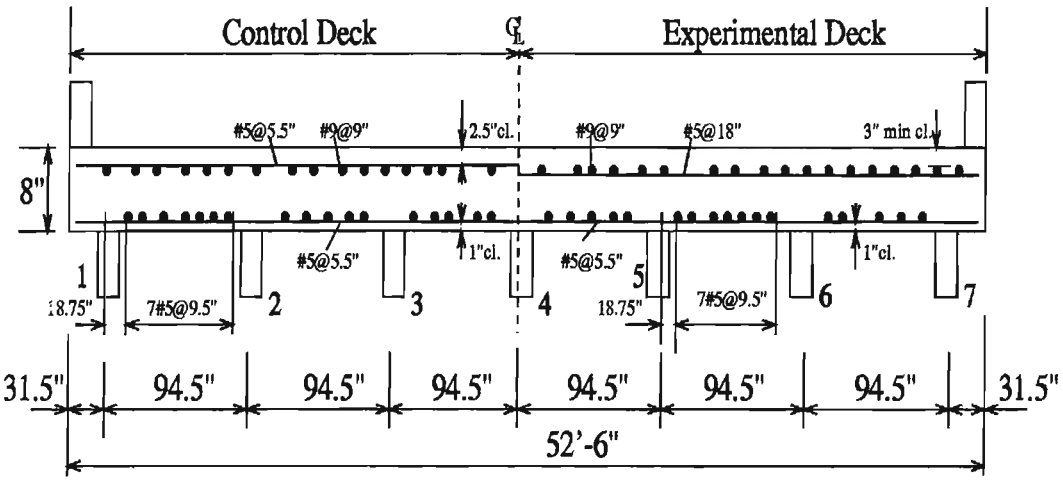

(b) Near Pier

Figure 2.2: Reinforcing Details for the Bridge Deck (Not to Scale

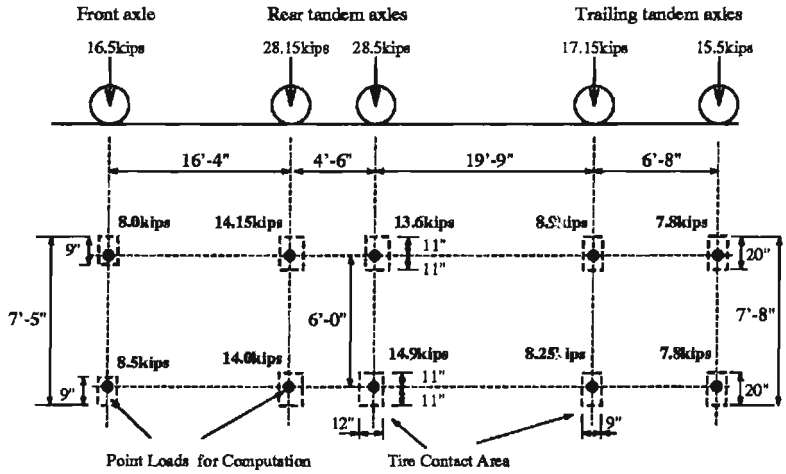

Figure 2.3: Test Truck (9/11/93)

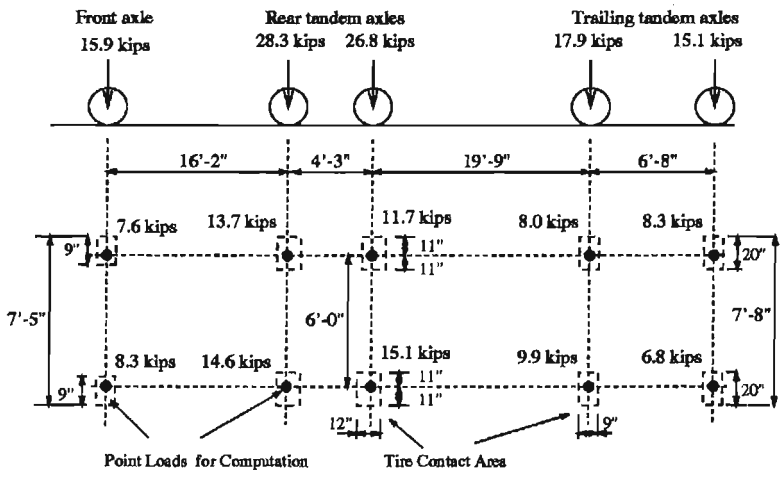

Figure 2.4: Test Truck (3/17/95)

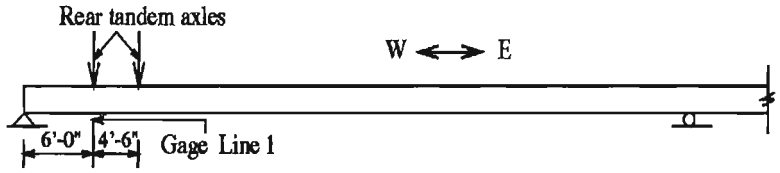

(a) Test Truck Near Abutment(Load Group 1)

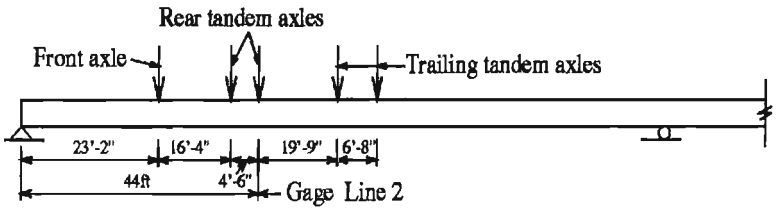

(b) Test Truck Near Mid-Span (Load Group 2)

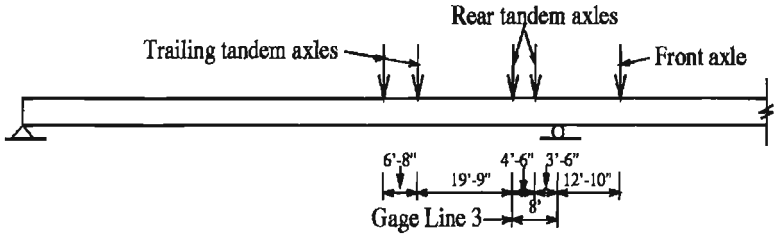

(c) Test Truck Near Pier (Load Group 3)

Figure 2.5: Longitudinal Positions of Test Truck on the Bridge

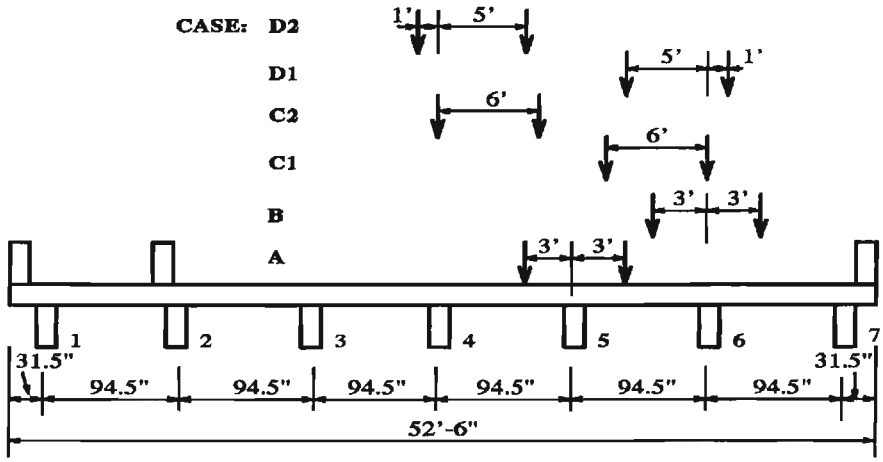

(a) Test Truck Near Abutment and Pier

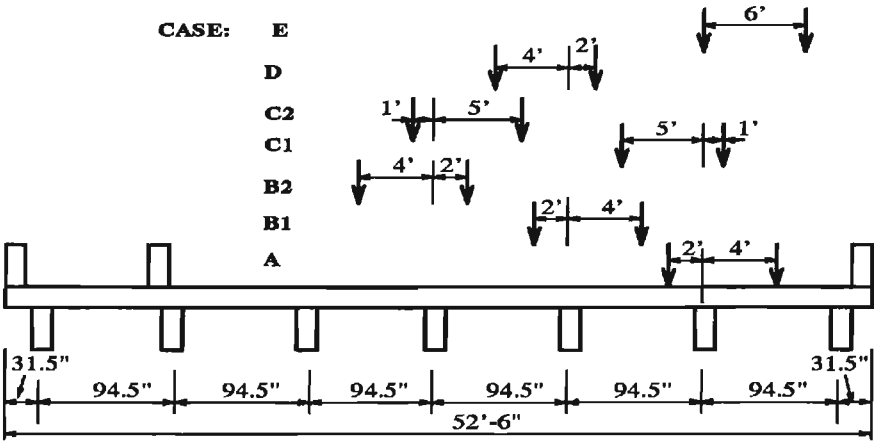

(b) Test Truck Near Mid-Span

Figure 2.6: Test Truck Positions along Transverse Direction of the Deck

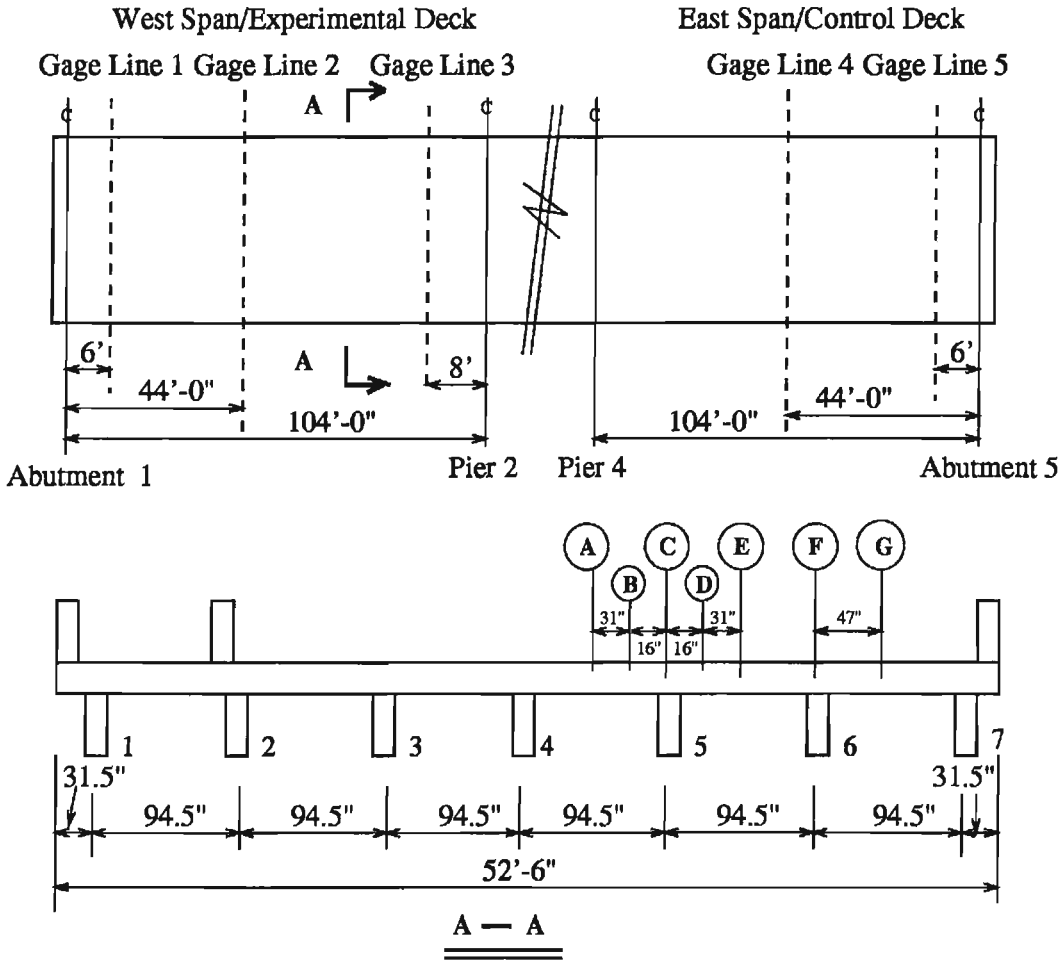

Figure 2.7: Locations of Strain Gages in the Bridge Deck

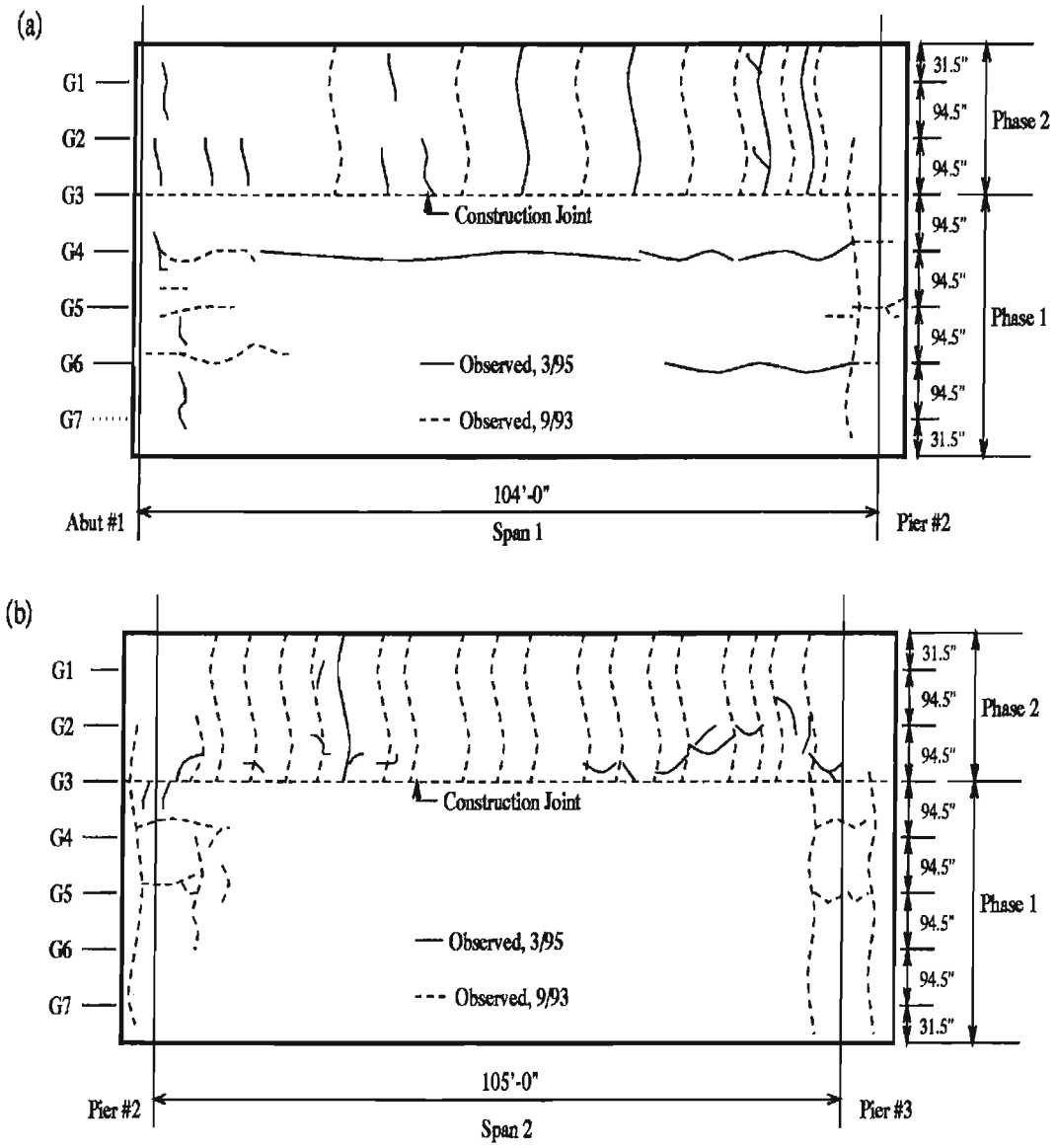

Figure 2.8: Approximate Sketch of the Pre-Test Cracking Pattern at the Top of the Deck: (a) Span 1; (b) Span 2.

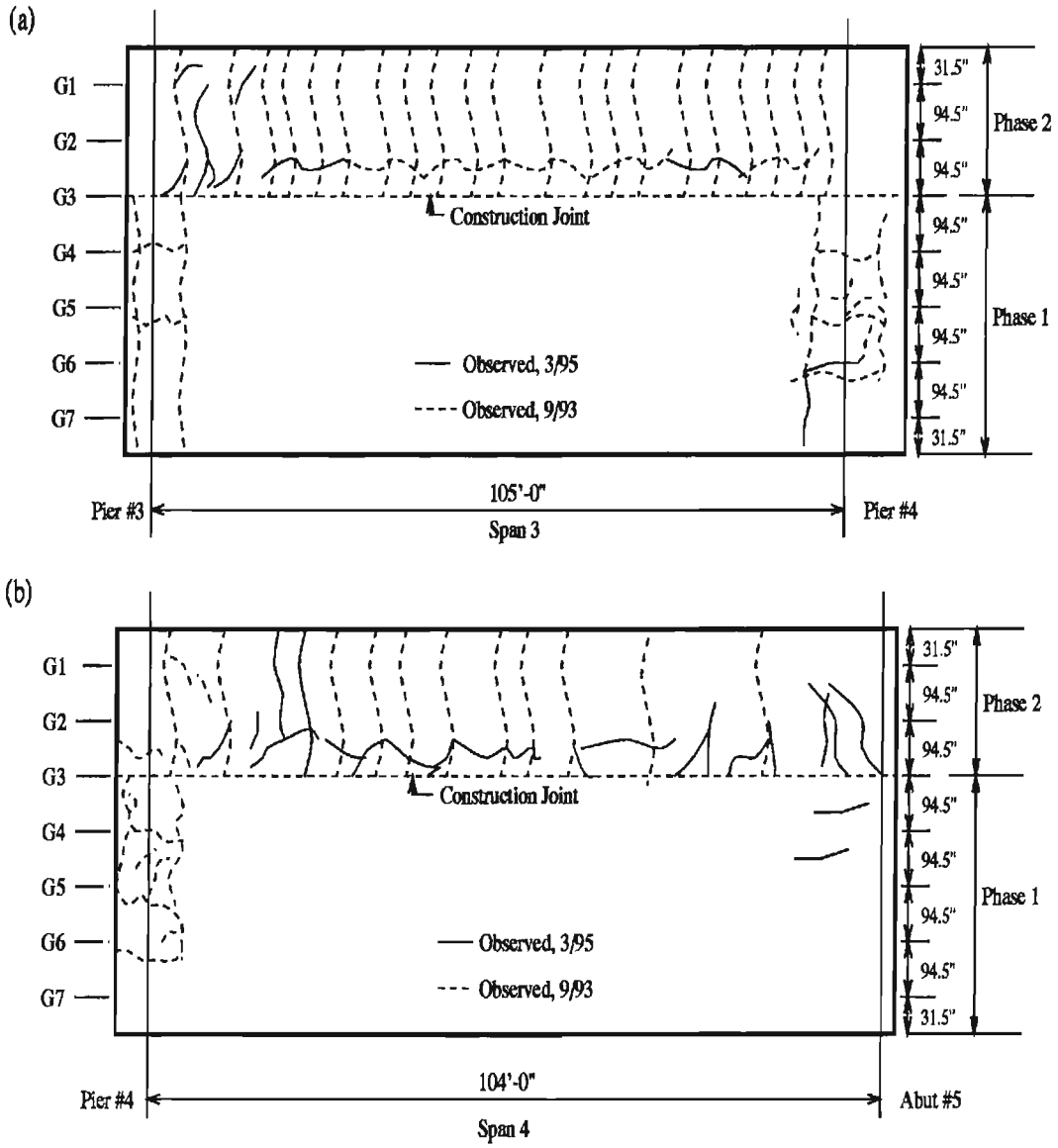

Figure 2.9: Approximate Sketch of the Pre-Test Cracking Pattern at the Top of the Deck: (a) Span 3; (b) Span 4.

Chapter 3

FINITE ELEMENT MODELING OF BRIDGE DECK

3.1 General Considerations

For the elastic stress analysis of a four-span bridge deck, it is impossible to use solid elements to model both the concrete slab and the girders due to the limitation of the computer capacity. Hence, in the finite element model adopted here, two layers of solid elements are used to model the concrete slab and rigid links are used to connect the nodes at the bottom of the slab to the centroids of the girders which are represented by 3-D beam elements. The cross-sectional area and moment of inertia of each girder of the bridge are 631 in^2 and 242,585 in^4, respectively. This modeling approach has been validated in a previous study (Cao, Allen and Shing 1993).

Furthermore, since only a single end span of the four-span bridge is considered at a time, the remaining three spans are modeled by equivalent beam elements only. Each equivalent beam has a 54-in-high and 43.45-in-wide rect

Table 3.1: Moment of Inertia of the Equivalent Beam

Components	$A_i(\text{in}^2)$	$I_i(\text{in}^4)$	$y_i(\text{in})$	$A_i y_i$	$Y_i(\text{in})$	$A_i Y_i^2$	$I_i + A_i Y_i^2$
Slab	756	4,032	4.0	3,024	13.95	147,120	151,152
Girder	631	242,585	34.67	21,877	16.72	176,401	418,986
Total	1,387	—	—	24,901	—	—	570,138

Note:
A_i — Area of the ith component of the composite section;
I_i — Moment of inertia of the ith component of the section;
y_i — Distance between the centroid of the ith component of the section and the top of the slab;
Y_i — Distance between the centroid of the ith component of the section and the neutral axis of the equivalent beam.

angular section, whose moment of inertia is equal to that of a fully-coupled composite T-beam section consisting of a girder and a concrete slab. The effective width of the flange is equal to the center-to-center distance between the girders, in accordance with ACI recommendations (ACI 1989). The moment of inertia of the equivalent beam is 570,138 in^4, as shown in Table 3.1.

In this study, the most important consideration is the maximum tensile stresses produced by transverse negative moments in the slab. These stresses are thought to occur at the top of the deck in the vicinity of supporting girders. Therefore, a suitable mesh should be chosen to obtain accurate stresses at these sites. The strategy used here to select a mesh is to vary element sizes in the longitudinal and transverse directions independently, and a suitable element size is determined by looking at the convergence of the stresses. The study on mesh refinement is documented in detail by Cao, Allen and Shing (Cao 1993), and is briefly summerized in the following paragraphs.

Table 3.2: Maximum Transverse Tensile Stresses with Different Meshes

Longitudinal Divisions	Element Aspect Ratio	Max. Tensile Stress (ksi)	% Error with Respect to 30 Elements
10 Elements	10.64	0.467	17.54
20 Elements	5.32	0.545	3.73
30 Elements	3.55	0.566	0.0

The mesh refinement study was carried out with a simply supported bridge deck that had a span length of 399 inches and seven equally spaced girders. The concrete slab was modeled with two layers of solid elements. The concrete slab between two girders is discretized into seven solid elements in the transverse direction of the deck. Furthermore, with the mesh in the transverse direction fixed, the slab was divided into 10, 20 and 30 elements, respectively, in the longitudinal direction. Such arrangements lead to element aspect ratios (length/thickness) of 10.64, 5.32 and 3.55, respectively.

With two 50-kip point loads applied at the mid-span of the deck, stresses were computed with the aforementioned meshes. The maximum transverse tensile stresses at the top of the deck obtained with the different meshes are compared in Table 3.2, where the maximum transverse tensile stress obtained with 30 elements is used as the comparison standard. Based on the results in Table 3.2, it is estimated with a quadratic interpolation that using an element aspect ratio not greater than 7.0 leads to an error less than 10%.

Furthermore, the simply supported bridge deck was discretized with two different meshes in the transverse direction. In both cases, there were 30 solid elements in the longitudinal direction of the deck. In the coarse mesh, there is only one solid element between a wheel load and a girder, and in the

fine mesh, two solid elements were used.

Analysis results obtained with the coarse mesh appear unrealistic in that the maximum stresses in the transverse direction do not occur under the point loads or above the girders. This means that stresses at these sites are greatly distorted. When the fine mesh is used, this distortion virtually disappears. Hence, it is apparent that there should be at least two solid elements between a wheel load and a girder for stress analysis. Based on these considerations, a mesh of eight elements in the transverse direction between each pair of girders has been chosen.

3.2 Finite Element Models

Based on the above considerations, only one end span is modeled in a refined fashion at a time. A total of 50 solid elements is used in the transverse direction of the bridge deck, with eight solid elements used between two girders. The span length between two girders is adjusted to be 96 inches, which is 1.5-in longer than the actual span length, to fit the different wheel load positions along the transverse direction. The mesh along the transverse direction remains the same for all three load groups. The mesh along the longitudinal direction is adjusted in accordance with the locations of the axle loads of the test truck. The dimensions of the test truck are slightly modified to fit the meshes. The distance between the rear tandem axles is changed from 54 to 48 inches. The length of the truck is modified to be 9-in shorter for Load Group 2, and 2-in shorter for Load Group 3 than the actual length of the test truck. A total of 24 solid elements is used in the longitudinal direction of a single span. For all three load groups, a fine mesh is used in the vicinity of the rear tandem axle loads. In this region, the

length of each element is 24 inches, which leads to an element aspect ratio (length/thickness) of 6.0. In the model, the span length of the bridge is 104 feet for the two end spans and 105 feet for other spans, which are equal to the actual span lengths of the bridge. The vertically supported joints are located along the central line of the diaphragm above the abutment or the pier.

The mesh used for the stress analysis of the deck under Load Group 1 is shown in Fig. 3.1(a). From the left side of the mesh, the first solid element has a length of 15 inches. This element accounts for the stiffness of the concrete diaphragm above the abutment. This effect is simulated by using equivalent solid elements which have the same in-plane bending stiffness as that of the diaphragm. The depth and width of the diaphragm are 62 and 30 inches, and those of the equivalent solid elements are 8 and 15 inches. Since the modulus of elasticity of the diaphragm is calculated to be 4,230 ksi, that of the equivalent solid elements is determined to be 279,560 ksi. In the longitudinal direction, six small solid elements are used in the region of the fine mesh, and the rest of the deck is modeled by seventeen solid elements.

The mesh used for the stress analysis of the deck under Load Group 2 is shown in Fig. 3.1(b). In the longitudinal direction, six small solid elements are used in the region of the fine mesh, and the rest of the deck is modeled with eighteen solid elements. The lengths of these elements vary so that the axle loads can be located at the desired nodes.

The mesh used for the stress analysis of the deck under Load Group 3 is shown in Fig. 3.1(c). There are two solid elements with a high modulus of elasticity (32,760 ksi) used to account for the stiffness of the diaphragm above the pier. The depth and width of the diaphragm are 62 and 51 inches, and those of the equivalent solid elements are 8 and 25.5 inches. The approach

used to determine the modulus of elasticity for the equivalent solid elements is the same as that for Load Group 1. In the longitudinal direction, twelve small solid elements are used in the region of the fine mesh, including two solid elements for the diaphragm, and the rest of the deck is modeled with twelve solid elements.

In the finite element analysis of the bridge, the elastic modulus for deck concrete is assumed to be 4,230 ksi and that for girder concrete is 5,260 ksi. The Poisson's ratio is assumed to be 0.2 for both the deck and girder concrete. There is a steel diaphragm consisting of a C15X33.9 channel at the middle of each span, whose cross-sectional area is 9.96 in^2. The diaphragm is modeled by bar elements which are connected to the girders. The elastic modulus of the bars is assumed to be 29,000 ksi.

The bridge deck has an eight-degree angle of skew. However, because the angle of skew is small, it is ignored in the stress analysis. The wheel loads of the test truck are treated as concentrated point loads, which are applied at appropriate nodes of the finite element mesh. The finite element program SAP90 (Wilson 1989) is used for the stress analysis. Non-conforming solid elements are used to eliminate possible shear locking.

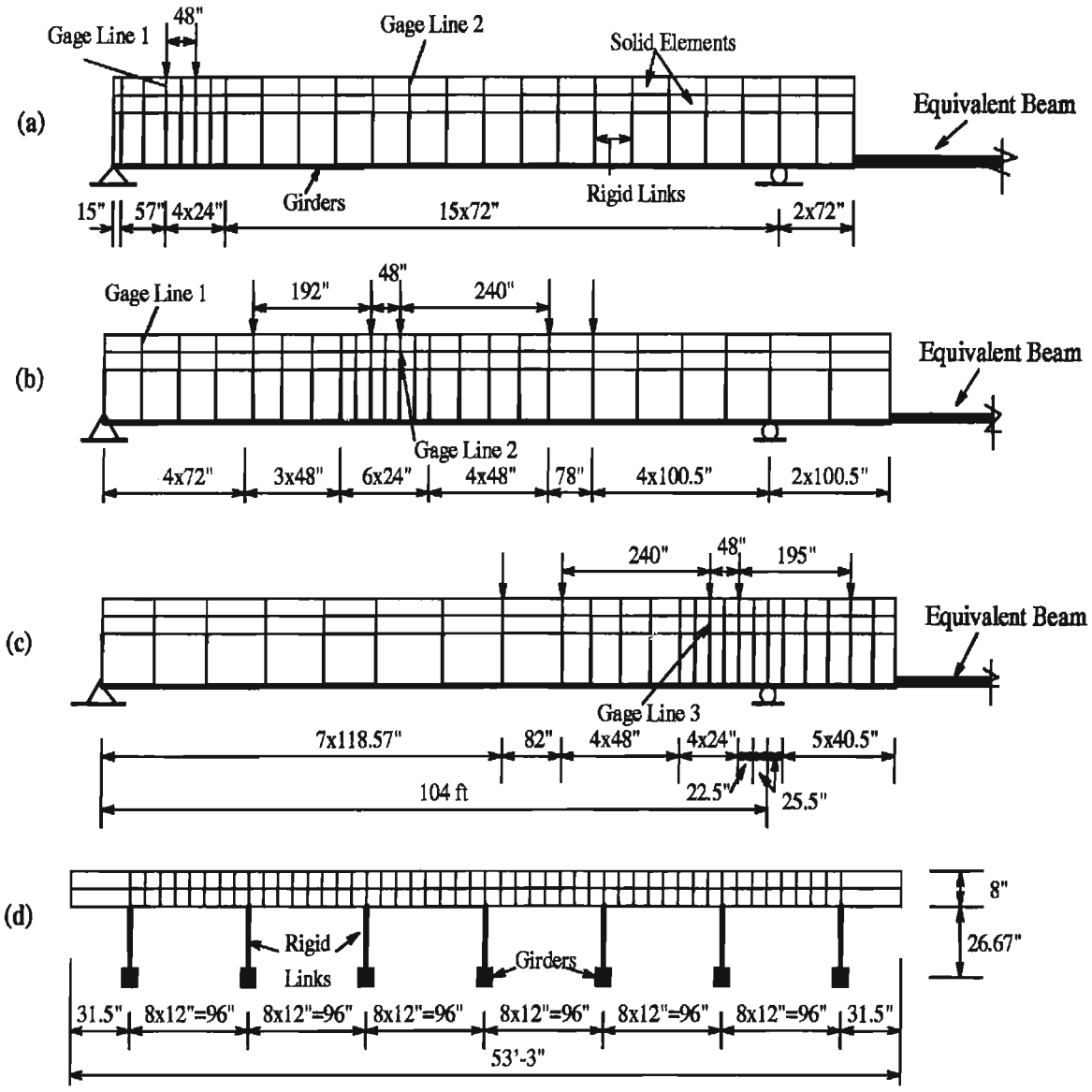

Figure 3.1: Finite Element Meshes: (a) Longitudinal Section for Load Group 1; (b) Longitudinal Section for Load Group 2; (c) Longitudinal Section for Load Group 3; (d) Transverse Section for All Three Load Groups.

Chapter 4

TEST AND NUMERICAL RESULTS

4.1 Results of Field Tests

The response of the bridge deck to the test trucks positioned at the different locations mentioned previously was measured by embedded strain gages. These strain readings obtained with the two series of load tests are tabulated in Appendix A. The maximum strain readings for the first series of load tests at the top and bottom of the deck are summarized in Tables 4.1 and 4.2. Those for the second series of load tests are summarized in Tables 4.3 and 4.4.

In the first series of load tests, when the test truck was close to the abutment, the maximum transverse tensile strains at the top gage positions of the deck along Gage Line 1 were less than 20×10^{-6} and those at the bottom gage positions of the deck were about $60\sim80\times10^{-6}$, as shown in Table 4.1. In the second series of load tests, the tensile strains at the top gage positions were less than 25×10^{-6} and those at the bottom gage positions were about $70\sim90\times10^{-6}$, as shown in Table 4.3.

Table 4.1: Maximum Values of Strain Readings ($\times 10^6$) in the Transverse Direction at Top/Bottom of Slab (9/11/93)

Gage Point	Gage Line				
	1	2	3	4	5
A	+3.1/+66.5	-52.3/+117.9	-53.3/+54.9	−/−	−/−
B	−/-31.5	-24.5/−	−/−	−/−	−/−
C	+20/−	+6.8/−	+19.2/−	+5.6/−	+13.8/−
D	+18.3/−	−/+50.7	−/−	−/−	−/−
E	-32.6/+76.7	-53.9/+173.8	-51.1/+73.4	-46.5/+133.2	-39.6/+30.2
F	+15.4/−	+13.0 /−	+18.7/−	−/−	+15.7/−
G	-14.8/+30.8	−/+176.2	−/−	−/−	−/−

Note: The plus and minus signs refer to the tensile and compressive strains, respectively. The locations of gage lines and gage points are illustrated in Fig. 5. The strain readings in each column are obtained under a load group which has the same number as the gage line.

When the test truck was near the mid-span for the first series of load tests, the transverse tensile strains at the bottom gage positions of the deck along Gage Line 2 were about $110\sim180\times10^{-6}$, and the transverse tensile strains at the top gage positions of the deck were less than 15×10^{-6}. In the second series of load tests, the tensile strains at the bottom gage positions were about $100\sim200\times10^{-6}$, and those at the top gage positions were less than 13×10^{-6}.

The longitudinal tensile strains developed in the deck under the test truck in the first series of load tests were less than 28×10^{-6} for all three load groups. Those in the second series of load tests were less than 27×10^{-6} for all three load groups.

Table 4.2: Maximum Values of Strain Readings ($\times 10^6$) in the Longitudinal Direction at Top/Bottom of Slab (9/11/93)

Gage Point	Gage Line				
	1	2	3	4	5
A	−/+0.4	-61.8/+1.0	-10.9/+10.7	−/-30.2	−/−
C	+6.2/−	-41.9/−	−/−	−/−	+10.0/−
E	-24.3/+27.5	-35.7/-23.4	−/−	−/-21.9	−/−
F	-17.3 /−	-51.7/−	−/−	−/−	−/−

Table 4.3: Maximum Values of Strain Readings ($\times 10^6$) in the Transverse Direction at Top/Bottom of Slab (3/17/95)

Gage Point	Gage Line				
	1	2	3	4	5
A	-19.1/+48.4	-38.1/+100.7	-54.4/+39.3	−/−	−/−
B	−/−	-28.0/−	−/−	−/−	−/−
C	+24.8/−	+8.5/−	+16.3/−	+9.7/−	+10.7/−
D	+22.8/−	−/+65.2	−/−	−/−	−/−
E	-30.1/+90.0	-58.9/+193.8	-42.7/+92.7	−/+148.9	-35.1/+26.9
F	+24.4/−	+12.8 /−	+18.1/−	−/−	+18.1/−
G	-12.3/+71.6	−/+158.2	−/−	−/−	−/−

Table 4.4: Maximum Values of Strain Readings ($\times 10^6$) in the Longitudinal Direction at Top/Bottom of Slab (3/17/95)

Gage Point	Gage Line				
	1	2	3	4	5
A	−/-11.9	-61.6/+1.2	+7.3/-12.6	−/-27.7	−/−
C	-18.2/−	−/−	−/−	−/−	+11.2/−
E	-11.7/+26.4	-55.8/-20.8	−/−	−/-22.7	−/−
F	-7.8 /−	-55.5/−	−/−	−/−	−/−

4.2 Comparison of Test and Numerical Results

The behavior of the bridge deck under the nineteen load cases is analyzed with the finite element models presented in Chapter 3. The corresponding normal stresses along the transverse and longitudinal directions of the bridge deck are determined.

Since two layers of 8-node solid elements have been used to model the bridge deck, the stresses have been computed at three nodal points along the depth of the slab. The stresses at the gage locations have been evaluated from the nodal stresses with a linear interpolation, which happens to fit the nodal stresses very well. In spite of the small variation of gage positions, it has been assumed that all strain gages are 1.0 inch away from the top or bottom of the deck. Since the normal strains in both the longitudinal and transverse directions were measured at most of the gage positions, the normal stresses in the deck have been calculated with a biaxial stress-strain relation, in which the modulus of elasticity and the Poisson's ratio of the deck concrete are the same as those used in the finite element model.

Finite element analysis were conducted with the wheel loads and spacing based on the test truck used in the first series of load tests. As shown in Fig. 2.3, the test truck included a front axle transmitting a force of 16.5 kips. The total force transmitted by the rear tandem axles of the test truck was 56.65 kips and the total forces exerted by the trailing axles was 32.75 kips. The total weight of the test truck was 106 kips, which is 47% more than a conventional HS20 truck. The axle and wheel spacings of the test truck were similar to those of a standard HS20 truck.

The comparisons of the test and numerical results on the normal stresses developed under different load groups are summarized in Appendices B and C. The test and numerical results from selected load cases are compared in Figs. 4.1 and 4.2. These correspond to Case A of Load Group 1 (Case 1A), and Case B1 of Load Group 2 (Case 2B1). The wheel load positions along the transverse direction of the deck are similar for these two cases, as shown in Fig. 2.6. These two load cases demonstrate the effect of girder deflection on the normal stresses in the transverse direction of the deck. It can be seen from the figures that the numerical results are quite close to the test results for these two cases. Nevertheless, the tensile stresses developed at the bottom of the deck in the field tests are about twice as large as the numerical predictions. This can be attributed to the cracking at the bottom of the deck, which is not accounted for in the analysis.

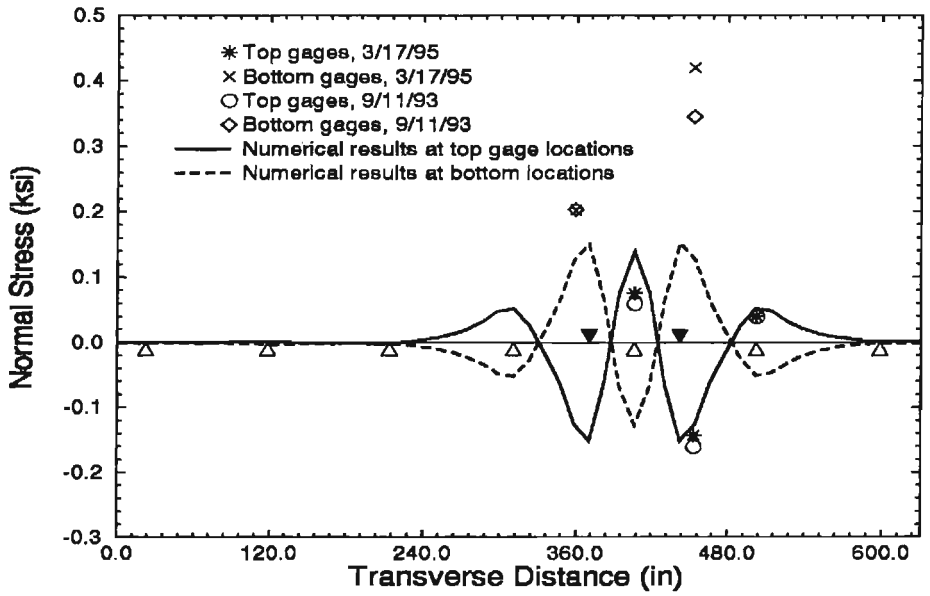

Figure 4.1: Normal Stress in Transverse Direction along Gage Line 1 (Case 1A)

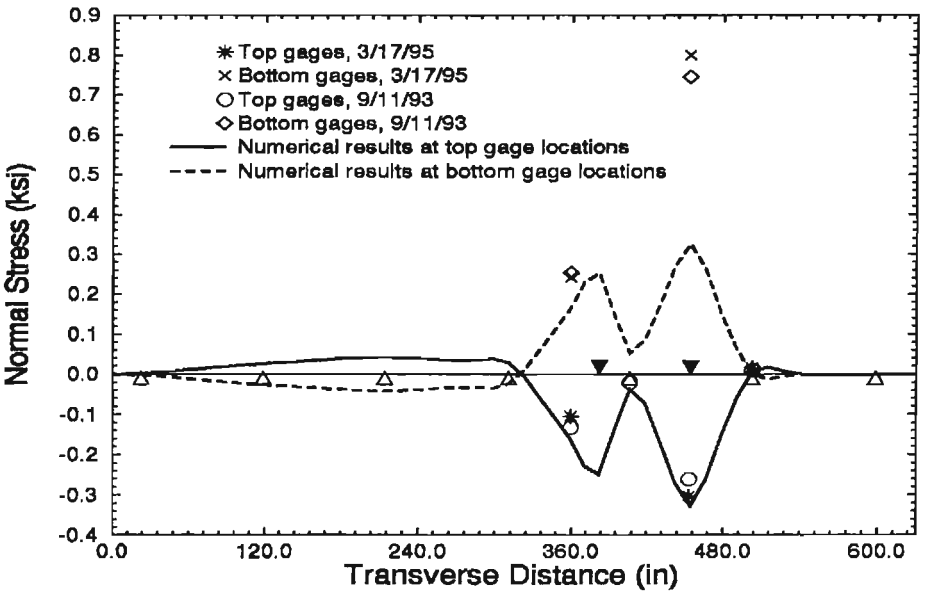

Figure 4.2: Normal Stress in Transverse Direction along Gage Line 2 (Case 2B1)

Chapter 5

SUMMARY AND CONCLUSIONS

5.1 Summary

The deterioration of a bridge deck due to the corrosion of top reinforcing bars could be prevented by eliminating the top reinforcement in the deck. This new concept was implemented in the design of an experimental deck in a four-span bridge, in which the top reinforcement was eliminated. To assess the maximum tensile stresses developed at the top of the deck under traffic loads, the behavior of the bridge deck was investigated with a test truck positioned at different locations. Two series of load tests were conducted.

The test trucks used for the first series and the second series of load tests weighed 106 and 104 kips, respectively, which are about 45% more than a conventional HS20 truck. The test truck was placed at three different longitudinal positions along the bridge for each series of load test. They were near the abutment, mid-span, and pier. When the test truck was near the abutment and the pier, the test truck was placed at six positions along the transverse direction. When the test truck was near the mid-span, the test

truck was placed at seven positions along the transverse direction. Therefore, there were totally nineteen truck positions on the bridge deck.

The response of the bridge deck under the test trucks was monitored with embedded strain gages during the two series of load tests. There were five designated gage lines along the longitudinal direction of the bridge. Three gage lines were located in the experimental deck of the bridge, and the other two gage lines were located in the control deck of the bridge. Along each gage line, there were seven gage points where gages were placed at the top and bottom of the deck along the transverse and longitudinal directions of the bridge.

It is found from the test results that when a truck load was near an abutment or a pier, the transverse tensile strains at the bottom of the deck were close to the cracking strain of deck concrete (140×10^{-6}). When a truck load was near a mid-span, the transverse tensile strains at the bottom of the deck exceeded the cracking strain. For all the load cases considered here, the transverse tensile strains at the top of the deck were always less than 40×10^{-6} which are much less than the cracking strain.

The behavior of the bridge deck under the three load groups has been analyzed with the finite element method. The numerical results have been compared with the test results. It is found that the numerical predictions of the deck response are close to the test results for the two series of load tests. When the test truck is near a mid-span of the bridge deck, the transverse tensile stresses at the top of the deck is very small due to girder deflections. For all three load groups considered here, the transverse tensile stresses at the top of the deck are only 30% of the modulus of rupture of deck concrete (590 psi), and are even less than the fatigue strength of deck concrete (355 psi).

5.2 Conclusions

From the experimental and numerical investigations of the response of a four-span slab-girder deck subjected to truck loads, the following conclusions have been reached.

1) From the test and numerical results, it has been found that the tensile stresses developed at the top of the deck are much less than the modulus of rupture of the deck concrete. They are also less than the fatigue strength of the deck concrete. Hence, it can be concluded that traffic loads alone are not sufficient to cause cracking at the top of the deck, since the normal truck loads are smaller than the designated truck loads used in the field tests and numerical analysis.

2) Results of this and prior studies indicate that top reinforcement is not necessary, except for the longitudinal reinforcement near an abutment or a pier. This can possibly slow down the deterioration of a deck due to the corrosion of top reinforcement.

3) There is no significant difference in performance observed from the results of the two series of field tests conducted approximately eighteen months apart.

For further studies, it will be informative to conduct non-linear stress analysis of the bridge deck, considering the cracking of concrete. Such studies will provide a better understanding of the behavior of concrete bridge decks under extreme traffic loads, as well as the effects of shrinkage and temperature cracks.

REFERENCES

ACI (1989). Building Code Requirements for Reinforced Concrete (ACI 318-89), American Concrete Institute.

Allen, J. H. (1991). "Cracking, Serviceability and Strength of Concrete Bridge Decks", Third Bridge Engineering Conference, *Transportation Research Record No. 1290*, Transportation Research Board, National Research Council, Washington, D.C., pp. 152-171.

AASHTO (1935). *Standard Specifications for Highway Bridges.* 2nd ed., American Association of State Highway and Transportation Officials, Washington, D.C.

AASHTO (1957–1961). *Minutes of AASHTO Bridge Subcommittee*, Federal Highway Administration Files, American Association of State Highway and Transportation Officials, Washington, D.C.

AASHTO (1992). *Standard Specifications for Highway Bridges.* 15th ed., American Association of State Highway and Transportation Officials, Washington, D.C.

Beal, D. B. (1982). "Load Capacity of Concrete Bridge Decks", *Journal of the Structural Division*, ASCE, Vol. 108, No. ST4, pp. 814-832.

Cao, L., Allen, J. H. and Shing, P. B. (1993). "A Case Study of Elastic Concrete Deck Behavior in a Four-Span Prestressed Girder Bridge: Finite Element Analysis", *Research Series No. CU/SR-93/1 (National Technical*

Information Service, #CDOT-DTD-CU-93-7), CEAE Department, University of Colorado at Boulder, January.

Cao, L., Allen, J. H., Shing, P. B. and Woodham, D. (1994). "A Case Study of Elastic Concrete Deck Behavior in a Four-Span Prestressed Girder Bridge: Correlation of Field Tests and Numerical Results", *Research Series No. CU/SR-94/4 (National Technical Information Service, #CDOT-DTD-CU-R-94-8)*, CEAE Department, University of Colorado at Boulder, April.

Fang, I. K., Worley, J. A., Burns, N. H. and Klingner, R. E. (1990). "Behavior of Isotropic R/C Bridge Decks on Steel Girders", *Journal of Structural Engineering*, ASCE, Vol. 116, No. 5, pp. 659-678.

Newmark, N. M. (1949). "Design of I-Beam Bridges", A Symposium of Highway Bridge Floors, *ASCE Transactions*, Vol. 114, pp. 979-1072.

USDOT (1989). " The Status of the Nation's Highways and Bridges: Conditions and Performance – *Highway Bridge Replacement and Rehabilitation Program*", U.S. Department of Transportation, Federal Highway Administration.

Westergaard, H. M. (1930). "Computations of Stresses in Bridge Slabs Due to Wheel Loads", *Public Roads*, March, pp. 1-23.

Wilson, E. L. et al. (1989). *SAP90 Program User's Manual*, Computers & Structures, Inc.

Appendix A

STRAIN GAGE READINGS FROM FIELD TESTS

The label of a strain gage as shown in the tables consists of four characters, which indicates its location and orientation. The first character of a gage label refers to the gage line number of the gage. The second character of a gage label refers to a gage point, which is the transverse position along a gage line. The third character of a gage label refers to the top or bottom position in a slab, with T denoting the top and B the bottom. The fourth character of a gage label refers to the gage orientation, with T denoting the transverse direction and L the longitudinal direction. An "X" appending to a label refers to an additional gage at the same location. For example, gage 2EBT refers to the strain gage located at gage point E of gage line 2, which is oriented in the transverse direction of the bridge and is at the bottom of the slab. The locations of gage lines and gage points are illustrated in Fig. 5. The load cases are illustrated in Figures 3 to 4. The negative strain readings refer to tensile strains, and the positive strain readings refer to compressive strains.

Table A.1: Strain Gage Readings ($\times 10^6$) under Load Group 1 (9/11/93)

Strain Gage	Load Case					
	A	B	C1	C2	D1	D2
1ATT	0.1	-3.1	-1.7	2.8	-2.8	2.8
1ABT	-46.2	-1.3	-0.3	-62.3	0.7	-66.5
1ABL	-0.2	0.0	-0.1	-0.2	-0.1	-0.4
1BBT	20.6	6.2	1.4	28.0	7.8	31.5
1CTT	-13.2	7.7	8.3	-20.0	5.6	-17.5
1CTL	-1.1	-6.2	-2.8	1.3	-5.5	1.6
1DTT	-18.3	-7.0	6.6	-3.1	-6.8	-2.5
1ETT	31.6	32.6	13.7	0.2	28.3	-0.1
1ETL	24.3	12.5	17.2	1.0	20.9	0.1
1EBT	-76.7	-72.8	-7.9	9.2	-69.0	8.3
1EBTX	-76.6	-72.9	-7.3	9.3	-68.2	8.3
1EBL	-7.9	27.5	3.5	1.8	11.7	0.9
1FTT	-10.0	-15.4	-11.2	-1.8	-9.4	-0.5
1FTL	5.9	15.5	17.3	-0.9	14.4	0.0
1GTT	-4.6	14.8	-8.6	-1.5	-4.8	-0.7
1GBT	6.8	-30.8	4.7	1.5	4.8	1.0
2ABL	-0.3	2.4	1.3	-0.3	1.8	-2.0
2CTT	-0.9	-5.1	-2.3	0.9	-4.3	0.5
2EBT	-11.1	-4.4	-12.5	-1.8	-9.1	-0.3
2EBL	-1.7	10.1	-4.5	1.1	-8.3	1.3
3ABL	-5.3	-6.9	-6.1	-3.1	-6.8	-3.0
3CTT	-7.9	-12.9	-9.9	-3.6	-12.5	-2.8
3EBT	-1.1	3.3	-0.7	-0.4	1.8	-0.4

Table A.2: Strain Gage Readings ($\times 10^6$) under Load Group 1 (3/17/95)

Strain Gage	Load Case					
	A	B	C1	C2	D1	D2
1ATTX	19.1	0.9	-0.4	12.3	-0.1	17.6
1ABTX	-48.4	0.6	6.6	-28.5	6.3	-45.2
1ABLX	11.9	5.4	8.6	-0.2	7.4	-11.6
1CTT	-20.5	-2.6	-4.3	-18.9	-4.8	-24.8
1CTL	16.9	3.0	5.3	17.6	5.1	18.6
1DTT	-22.8	-13.8	-5.0	-3.4	-14.7	-3.9
1ETT	30.1	21.1	11.9	1.8	21.8	2.0
1ETLX	11.7	-2.9	0.2	-2.9	-2.7	-1.9
1EBT	-88.1	-46.3	-18.6	13.3	-65.3	14.3
1EBTX	-90.0	-48.6	-19.7	11.5	-65.6	12.0
1EBLX	-26.4	26.3	10.4	6.8	14.0	8.3
1FTT	-9.5	-24.4	-6.4	-1.0	-13.4	1.1
1FTL	2.6	7.7	7.8	-2.4	6.8	-0.2
1GTT	-9.6	12.3	-11.0	-7.5	-8.2	-5.5
1GBT	10.3	-71.6	5.5	4.8	3.2	3.5
2ABL	-0.6	-0.3	-0.2	-0.5	-0.1	-0.9
2CTT	3.7	0.5	2.1	4.9	0.9	5.1
2EBTX	-11.7	-7.9	-12.5	-2.8	-10.6	-3.2
2EBL	8.7	7.3	8.1	10.4	8.1	11.4
3ABL	2.2	2.4	2.9	5.0	2.6	6.5
3CTTX	0.5	-0.9	0.2	2.3	-0.1	2.6
3EBT	-0.2	0.5	-0.2	1.5	0.3	0.4

Table A.3: Strain Gage Readings ($\times 10^6$) under Load Group 2 (9/11/93)

Strain Gage	Load Case						
	A	B1	B2	C1	C2	D	E
1CTT	9.0	12.4	-3.1	10.2	2.2	10.8	3.6
1EBT	-1.0	-5.6	3.0	-7.8	1.8	-1.2	1.3
1EBL	-1.5	-9.1	-6.6	-8.7	-8.9	-6.6	-0.1
2ATTX	-8.9	22.8	20.4	-6.6	52.3	51.9	-8.8
2ATL	22.9	36.7	36.0	20.1	48.3	61.8	15.5
2ABTX	17.3	-59.2	-46.7	4.3	-117.9	-117.0	19.8
2ABL	0.0	0.0	-0.3	0.4	-0.3	-1.0	0.4
2BTT	-7.6	24.5	-8.8	-4.1	3.1	9.4	-10.2
2CTT	-4.1	-3.9	-5.2	-6.8	-3.8	-5.5	-3.5
2CTL	26.1	41.9	28.6	23.2	36.5	38.4	18.3
2DBT	15.0	-15.7	-1.3	-7.2	-12.0	-50.7	14.5
2ETT	24.4	53.9	-6.0	44.3	-1.9	20.3	-5.2
2ETTX	23.4	52.6	-6.3	43.1	-2.3	19.4	-4.9
2ETL	35.3	33.7	18.2	35.7	22.7	31.3	21.8
2EBT	-66.2	-173.8	11.0	-142.1	-3.2	-82.3	5.3
2EBTX	-62.6	-160.8	9.4	-131.2	-3.9	-75.4	4.9
2EBL	21.0	22.6	13.7	14.3	14.3	20.3	23.4
2FTT	-8.0	-10.0	-6.8	4.8	-7.4	-13.0	-1.4
2FTL	51.7	39.1	17.1	44.7	21.9	28.1	33.4
2GBT	-176.2	5.8	21.0	-68.7	21.8	15.3	-93.3
3ABL	-2.1	-8.0	-10.1	-6.3	-11.5	-10.4	-0.2
3CTT	-4.4	-8.4	-5.4	-8.5	-7.5	-9.3	-3.9
3EBT	-9.1	-14.4	8.0	-17.3	4.9	-10.3	-4.2

Table A.4: Strain Gage Readings ($\times 10^6$) under Load Group 2 (3/17/95)

Strain Gage	Load Case						
	A	B1	B2	C1	C2	D	E
1CTT	10.2	11.4	-3.6	10.7	1.0	7.1	7.6
1EBT	-2.6	-8.8	2.6	-7.2	1.1	-4.6	3.4
1EBTX	-1.9	-8.4	2.3	-6.5	0.6	-5.0	4.3
1EBLX	-5.8	-9.5	-4.6	-6.7	-7.4	-9.3	-2.2
2ATTX	-7.5	16.2	15.3	-6.3	38.1	36.9	-9.3
2ATL	18.8	38.0	37.0	24.0	45.5	61.6	12.1
2ABTX	6.0	-55.2	-42.2	-3.6	-100.7	-87.8	11.0
2ABL	-0.5	0.4	-1.0	-0.3	-1.2	-1.2	-0.4
2BTT	-6.2	28.0	-12.0	-1.1	2.5	14.8	-10.3
2CTT	-4.1	-5.3	-8.5	-6.5	-6.7	0.2	-4.0
2DBT	17.1	-17.9	-1.1	5.0	-16.2	-65.2	20.3
2ETT	17.8	58.9	-8.8	53.5	-5.1	15.5	-5.6
2ETL	33.5	48.8	21.4	55.8	25.4	35.2	22.3
2EBTX	-62.2	-193.8	13.4	-175.8	-5.9	-64.0	5.8
2EBT	-60.0	-182.4	12.1	-165.5	-6.7	-60.2	4.1
2EBL	13.4	3.7	18.3	-7.2	20.8	20.8	18.4
2FTT	-8.8	-12.8	-8.1	-5.5	-9.5	-10.1	-5.3
2FTL	55.5	45.4	18.4	49.8	22.4	31.5	37.0
2GBT	-158.2	4.1	20.7	-74.9	20.9	15.4	-84.7
3ABL	-5.9	-9.3	-8.5	-6.3	-10.4	-11.1	-5.0
3CTTX	-0.4	7.2	5.0	1.7	7.3	8.2	-3.4
3EBT	-11.7	-19.3	8.1	-20.5	1.7	-12.9	-4.9

Table A.5: Strain Gage Readings ($\times 10^6$) under Load Group 3 (9/11/93)

Strain Gage	Load Case					
	A	B	C1	C2	D1	D2
1EBT	0.4	0.0	-1.2	-2.1	0.3	-0.5
1EBL	2.0	1.4	1.5	-0.2	1.7	1.1
2ABL	0.0	-0.1	0.3	0.0	-0.3	0.5
2CTT	2.7	1.7	2.3	0.0	2.6	0.3
2EBT	-12.0	-11.8	-13.5	-6.1	-13.9	-2.3
2EBL	1.7	-2.2	3.7	-0.4	1.1	1.9
3ATT	53.3	-3.8	-3.5	36.8	-6.2	48.0
3ATL	10.9	-0.5	-0.9	8.9	-0.2	-1.0
3ABTX	-54.9	6.1	7.1	-29.4	8.1	-43.1
3ABL	-10.7	-0.9	0.4	2.3	0.1	15.2
3CTT	-19.2	-3.6	-1.4	-6.2	-6.7	-10.9
3CTTX	-17.6	-4.0	-1.5	-4.8	-7.2	-9.1
3ETT	36.0	51.1	24.8	-3.2	42.0	-1.7
3EBT	-66.3	-72.9	-33.0	16.4	-73.4	17.3
3FTT	-3.8	-18.7	3.6	1.2	-7.1	2.7

Table A.6: Strain Gage Readings ($\times 10^6$) under Load Group 3 (3/17/95)

Strain Gage	Load Case					
	A	B	C1	C2	D1	D2
1EBTX	1.6	6.0	2.7	0.4	4.5	0.0
1EBLX	-7.0	-1.4	-8.1	-3.4	-5.3	-3.6
2ABL	-0.2	0.0	0.3	0.0	0.4	0.0
2CTT	0.0	0.3	1.0	-0.4	1.0	-0.4
2EBT	-8.8	-1.7	-9.5	-4.5	-5.7	-4.1
2EBL	1.2	2.5	1.8	1.4	2.6	1.5
3ATT	9.0	54.4	-0.3	24.2	36.4	43.9
3ATL	-5.6	-7.3	-3.2	3.8	-5.1	3.3
3ABTX	-35.7	8.1	8.4	-17.8	10.3	-39.3
3ABL	12.6	-1.9	-0.5	-1.1	-0.5	0.8
3CTT	-18.5	-3.1	-5.3	-10.9	-6.1	-13.3
3CTTX	-16.3	-2.3	-4.6	-9.7	-4.9	-12.0
3ETT	41.8	38.9	24.9	-1.7	42.7	-1.9
3EBT	-89.9	-58.4	-46.2	16.3	-92.7	16.0
3FTT	-7.9	-18.1	-2.0	1.4	-10.4	1.8

Table A.7: Strain Gage Readings ($\times 10^6$) under Load Group 4 (9/11/93)

Strain Gage	Load Case						
	A	B1	B2	C1	C2	D	E
4ABL	12.7	24.1	24.8	17.2	30.2	22.1	9.0
4CTTX	-2.7	-1.5	-5.6	-1.6	-5.2	0.2	-5.0
4ETT	28.2	46.5	-7.1	40.1	-4.3	25.3	-4.5
4EBT	-78.1	-133.2	11.3	-118.6	1.2	-79.8	0.7
4EBL	18.2	18.3	18.4	13.6	21.9	17.0	16.8
5CTTX	-4.4	3.1	8.5	-2.9	9.3	7.7	-7.5
5CTL	-0.2	-7.8	-6.2	-3.3	-8.1	-6.6	0.7
5ETT	5.8	9.8	1.1	8.5	3.1	8.4	-2.1
5EBTX	-5.1	-2.0	3.3	-3.9	3.6	-1.3	-4.6
5FTT	8.4	14.1	4.7	11.2	5.9	12.8	-0.6

Table A.8: Strain Gage Readings ($\times 10^6$) under Load Group 4 (3/17/95)

Strain Gage	Load Case						
	A	B1	B2	C1	C2	D	E
4ABL	14.0	23.7	23.3	18.6	27.7	25.7	8.3
4CTTX	-7.7	-0.5	-4.1	-4.2	-3.5	3.2	-9.7
4EBT	-78.5	-148.9	15.0	-146.1	-6.6	-89.8	1.3
4EBL	18.6	17.2	19.8	9.0	22.7	18.6	15.5
5CTTX	-15.0	0.3	9.6	-9.7	9.9	4.7	-19.9
5CTL	-4.8	-4.7	-2.3	-4.1	-4.1	-4.7	-5.7
5ETT	-0.7	9.2	1.3	5.1	4.1	8.8	-9.9
5EBTX	-5.3	-5.3	3.1	-6.6	1.2	-4.3	-4.4
5FTT	-0.6	13.8	6.3	8.1	8.9	12.4	-12.6

Table A.9: Strain Gage Readings ($\times 10^6$) under Load Group 5 (9/11/93)

Strain Gage	Load Case					
	A	B	C1	C2	D1	D2
4ABL	2.5	3.1	1.7	1.0	3.3	1.7
4CTTX	0.9	0.8	1.0	0.9	0.3	-0.2
4ETT	2.4	3.2	3.5	0.8	3.0	0.0
4EBT	-6.2	-5.2	-9.3	-3.8	-6.5	-2.7
4EBL	2.3	2.1	1.0	0.7	2.3	1.3
5CTTX	-13.8	-6.7	-9.4	0.0	-12.0	-1.5
5CTL	6.4	1.7	5.1	10.0	2.7	8.0
5ETT	39.6	26.5	19.4	1.2	32.3	-0.5
5EBTX	-30.2	-15.2	-14.3	1.9	-24.7	2.6
5FTT	-3.5	-15.7	-2.1	3.5	-10.3	2.4

Table A.10: Strain Gage Readings ($\times 10^6$) under Load Group 5 (3/17/95)

Strain Gage	Load Case					
	A	B	C1	C2	D1	D2
4ABL	2.2	0.5	1.7	2.6	2.2	2.4
4CTTX	1.5	-0.7	1.6	0.6	0.4	-0.3
4EBT	-8.7	-6.1	-8.7	-1.6	-6.5	-1.3
4EBL	1.3	-0.8	0.6	2.7	0.9	2.3
5CTTX	-10.7	-6.1	-6.9	-0.5	-9.2	-2.3
5CTL	11.2	0.8	6.9	9.9	4.7	10.4
5ETT	35.1	25.6	18.0	1.4	25.2	-0.6
5EBTX	-26.9	-20.5	-12.0	4.2	-22.3	3.6
5FTT	0.2	-18.1	2.0	3.1	-4.5	2.1

Appendix B

COMPARISON OF TEST AND NUMERICAL RESULTS FOR LOAD GROUP 1

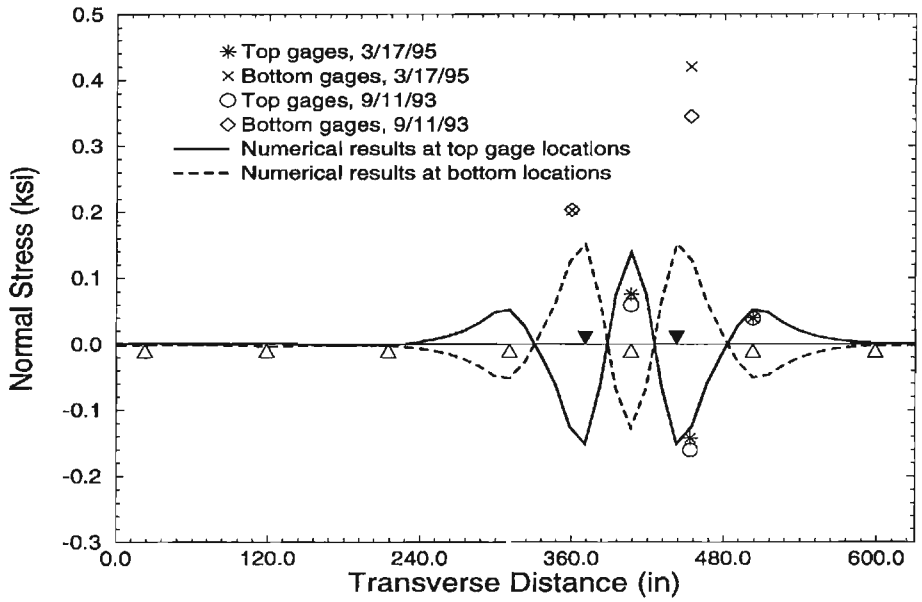

Figure B.1: Normal Stress in Transverse Direction along Gage Line 1 (Case 1A)

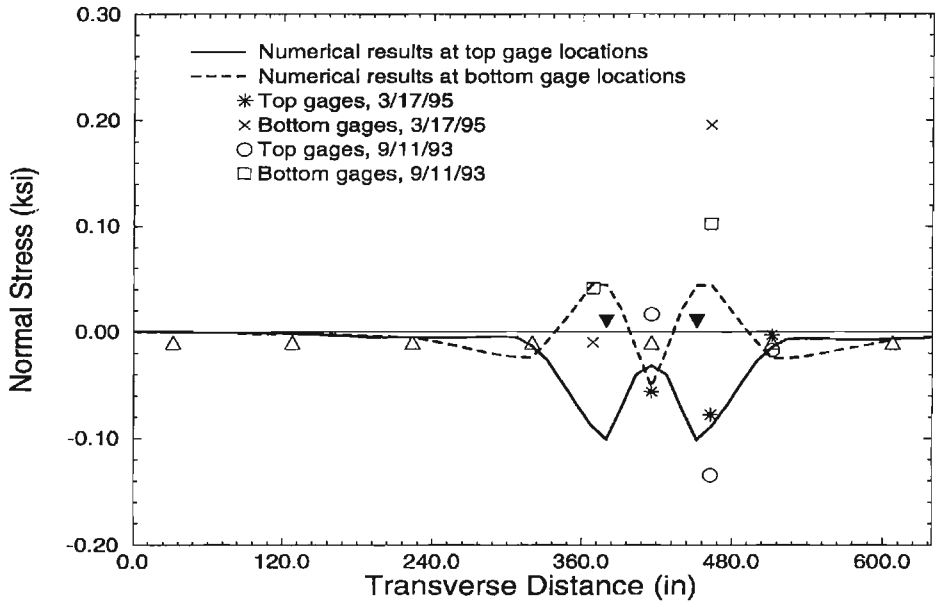

Figure B.2: Normal Stress in Longitudinal Direction along Gage Line 1 (Case 1A)

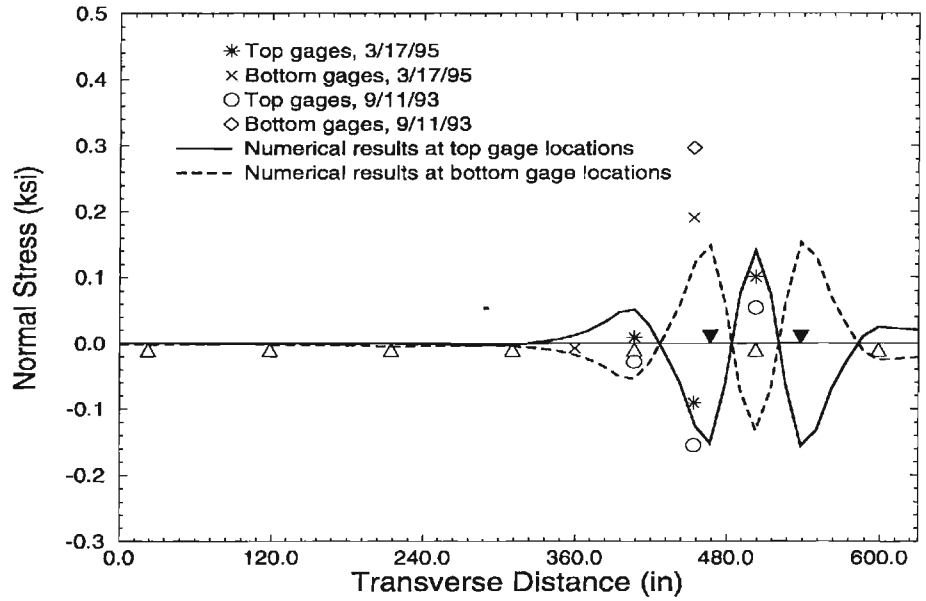

Figure B.3: Normal Stress in Transverse Direction along Gage Line 1 (Case 1B)

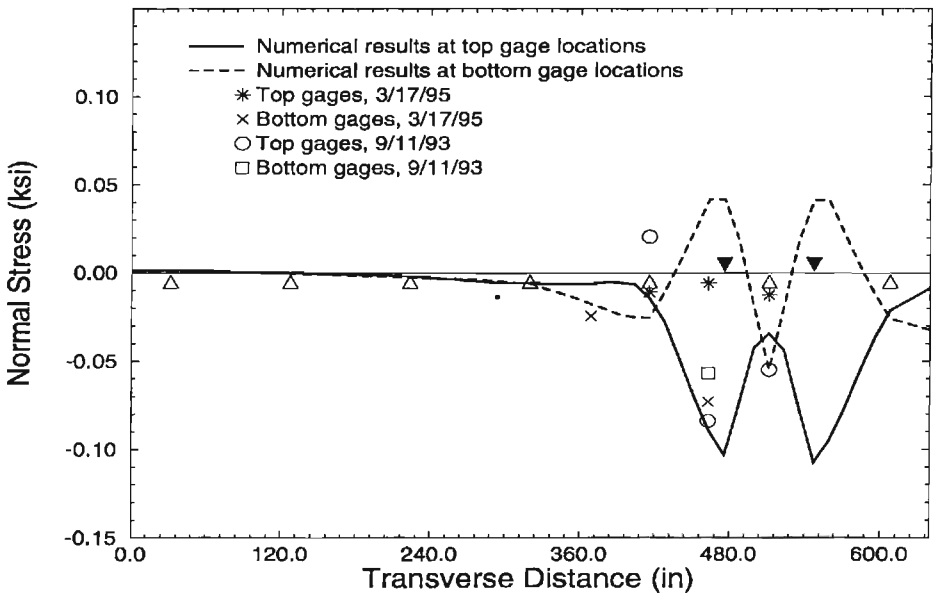

Figure B.4: Normal Stress in Longitudinal Direction along Gage Line 1 (Case 1B)

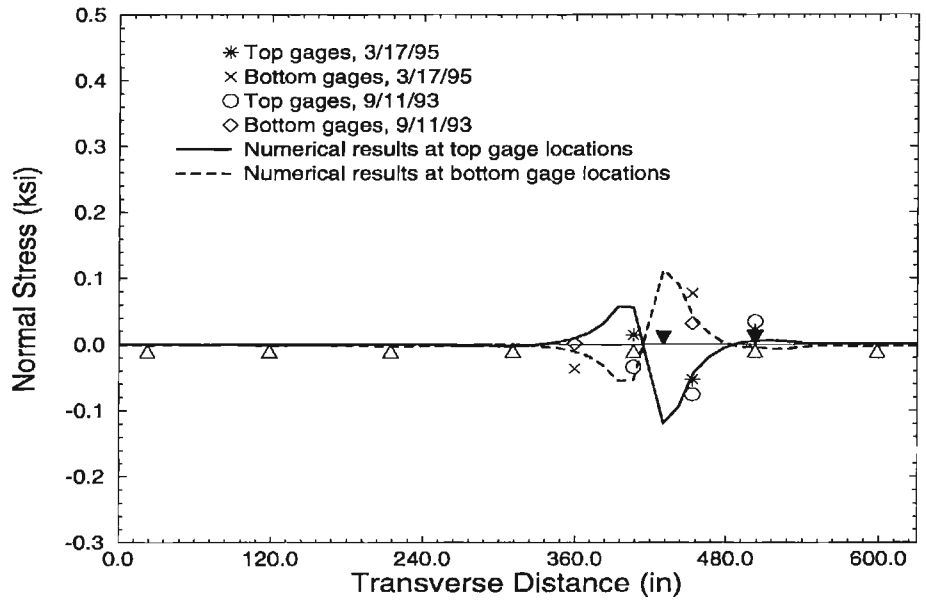

Figure B.5: Normal Stress in Transverse Direction along Gage Line 1 (Case 1C1)

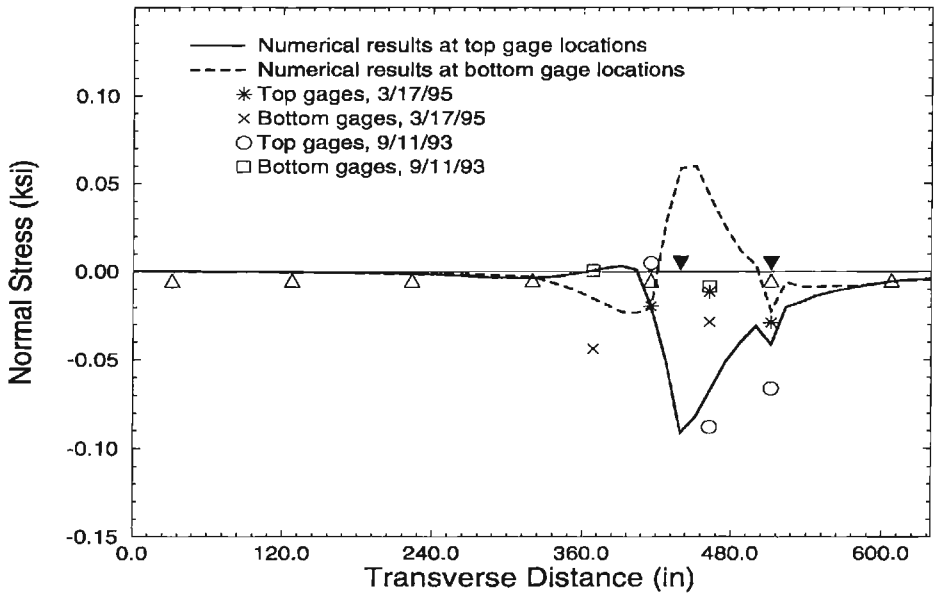

Figure B.6: Normal Stress in Longitudinal Direction along Gage Line 1 (Case 1C1)

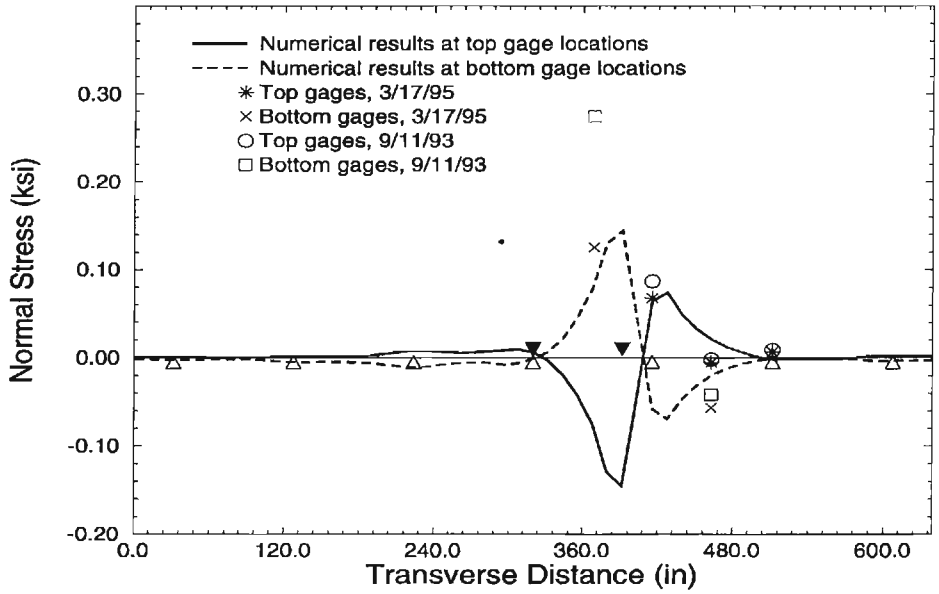

Figure B.7: Normal Stress in Transverse Direction along Gage Line 1 (Case 1C2)

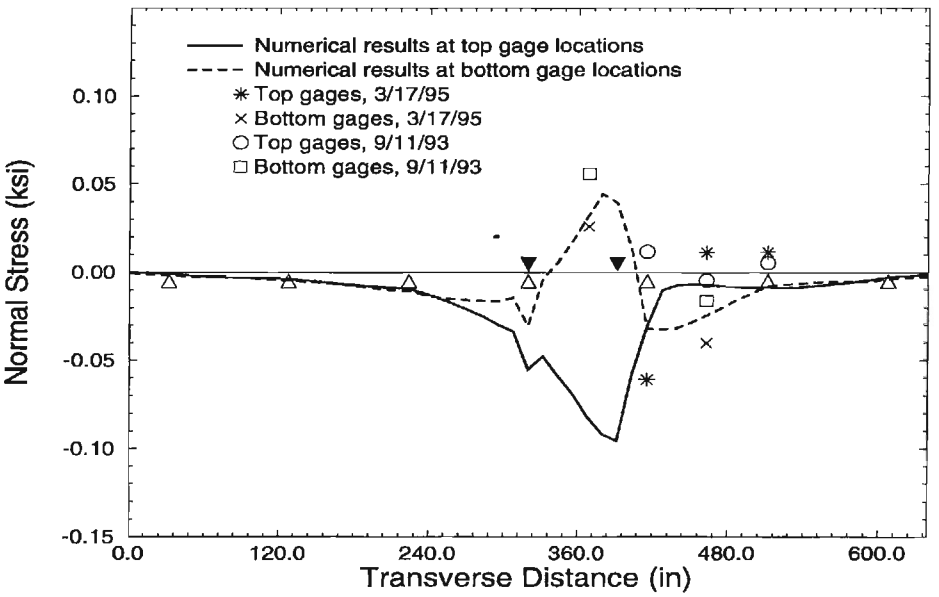

Figure B.8: Normal Stress in Longitudinal Direction along Gage Line 1 (Case 1C2)

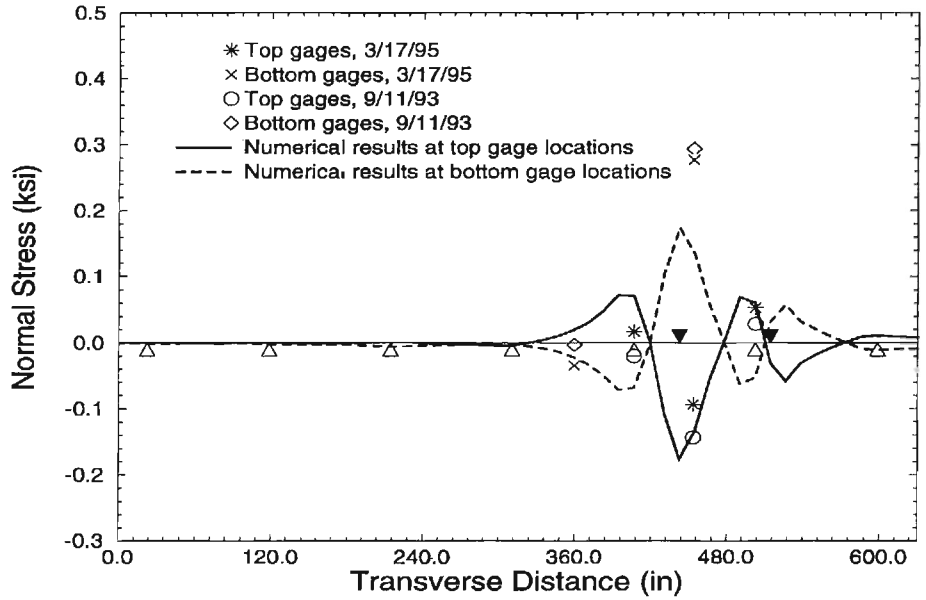

Figure B.9: Normal Stress in Transverse Direction along Gage Line 1 (Case 1D1)

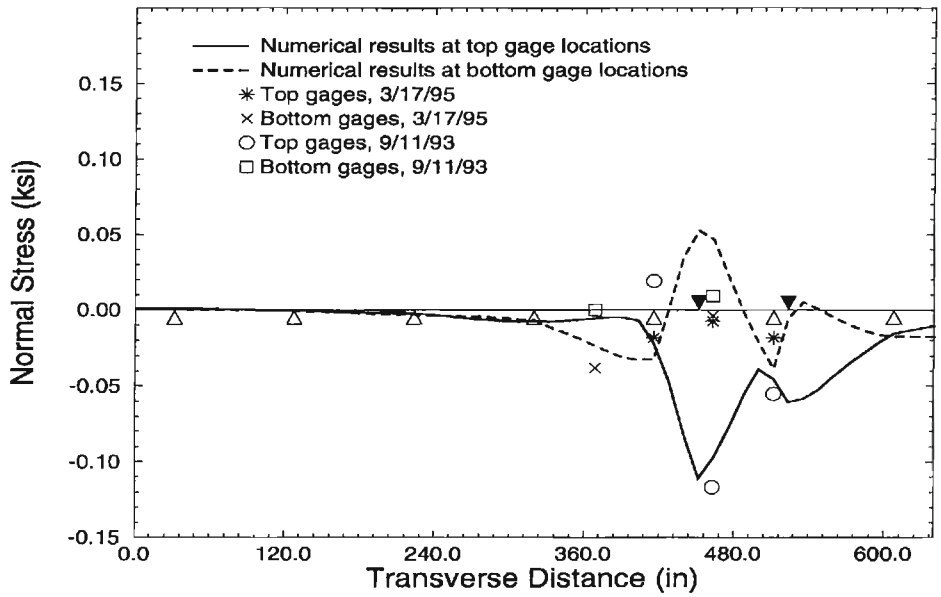

Figure B.10: Normal Stress in Longitudinal Direction along Gage Line 1 (Case 1D1)

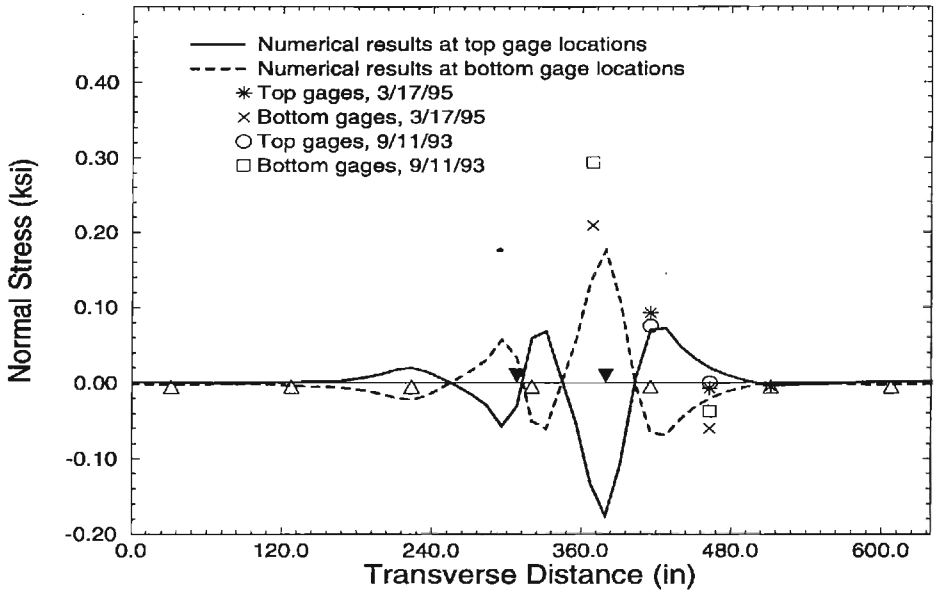

Figure B.11: Normal Stress in Transverse Direction along Gage Line 1 (Case 1D2)

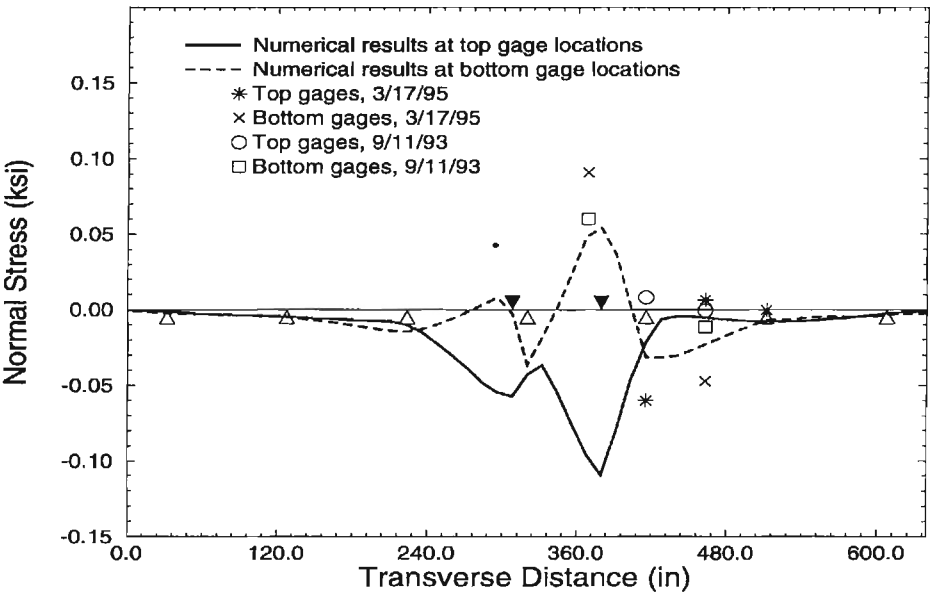

Figure B.12: Normal Stress in Longitudinal Direction along Gage Line 1 (Case 1D2)

Appendix C

COMPARISON OF TEST AND NUMERICAL RESULTS FOR LOAD GROUP 2

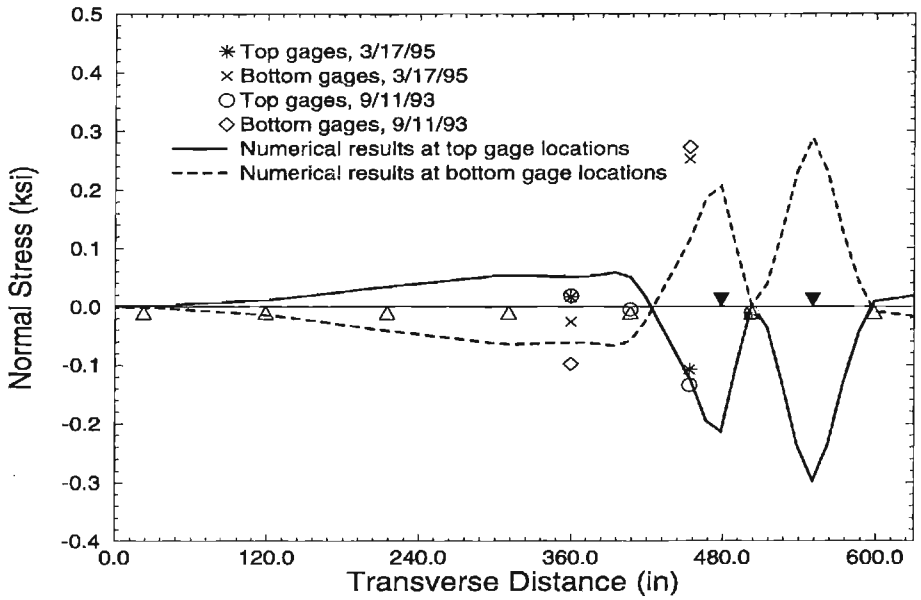

Figure C.1: Normal Stress in Transverse Direction along Gage Line 2 (Case 2A)

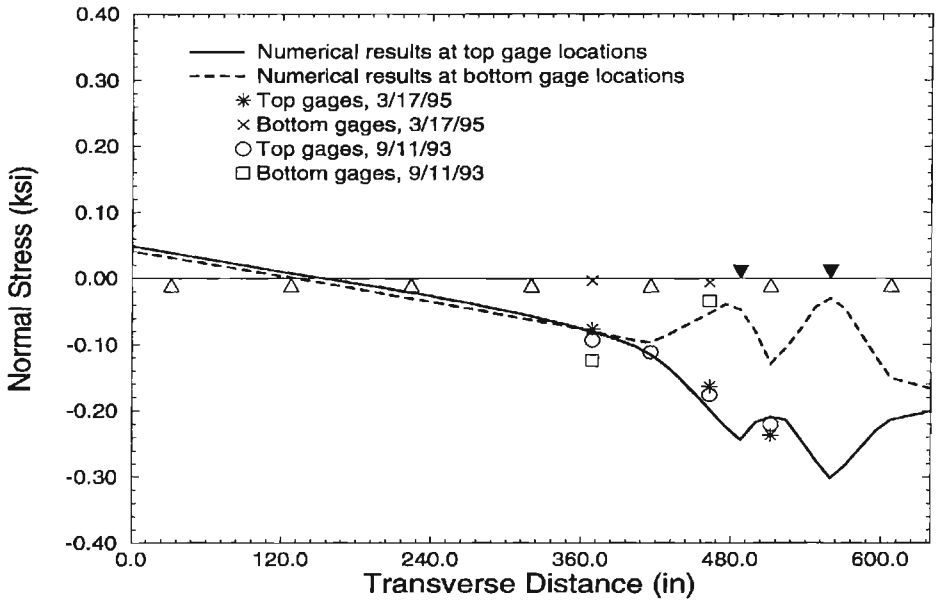

Figure C.2: Normal Stress in Longitudinal Direction along Gage Line 2 (Case 2A)

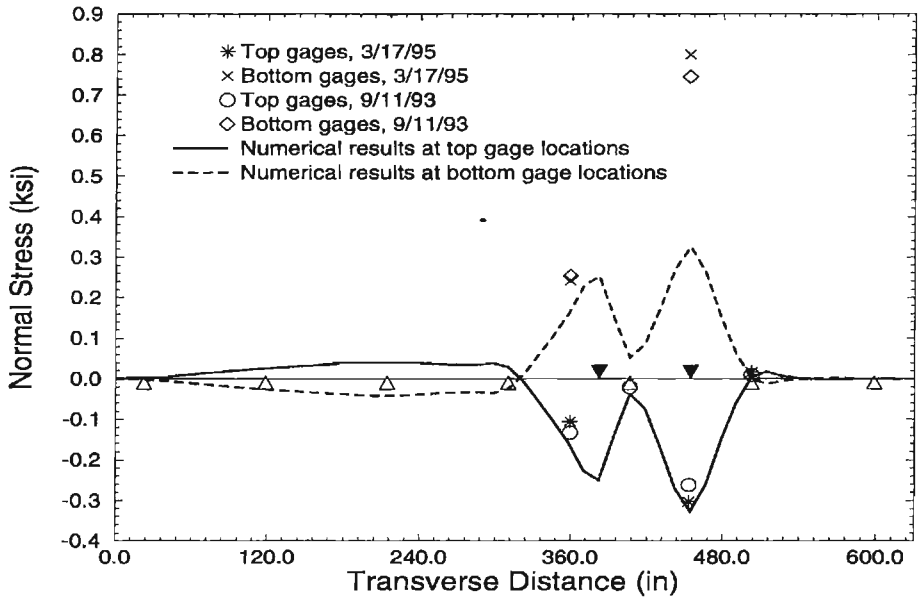

Figure C.3: Normal Stress in Transverse Direction along Gage Line 2 (Case 2B1)

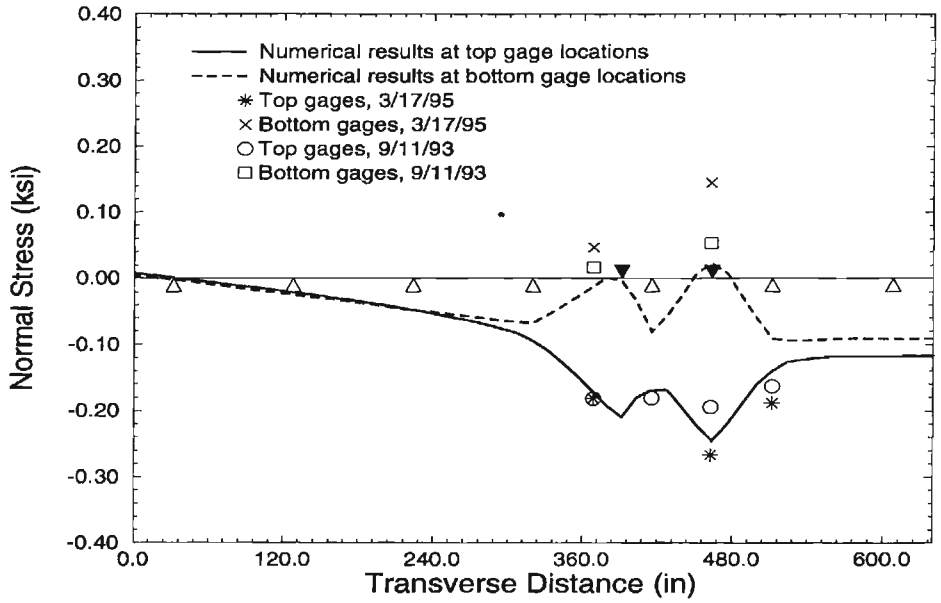

Figure C.4: Normal Stress in Longitudinal Direction along Gage Line 2 (Case 2B1)

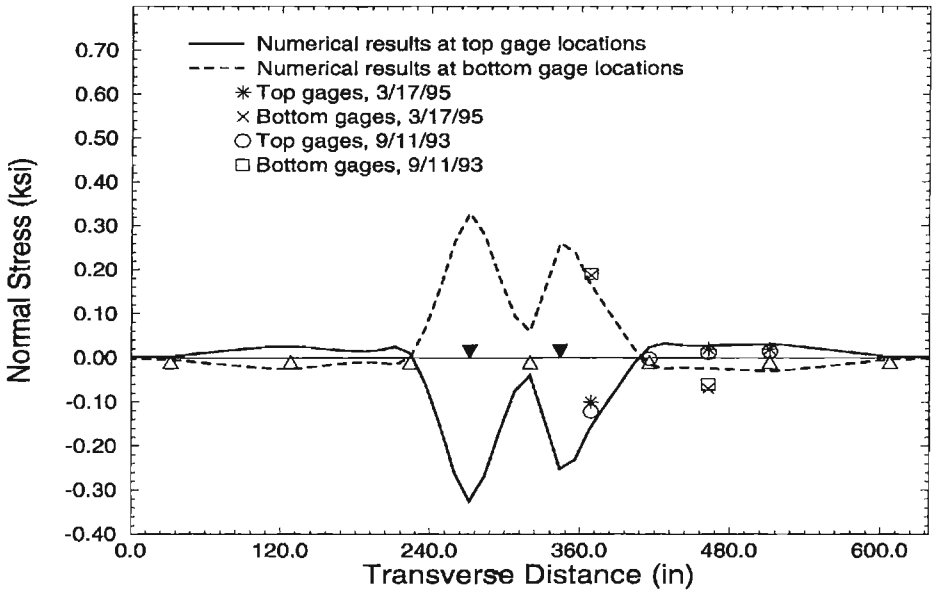

Figure C.5: Normal Stress in Transverse Direction along Gage Line 2 (Case 2B2)

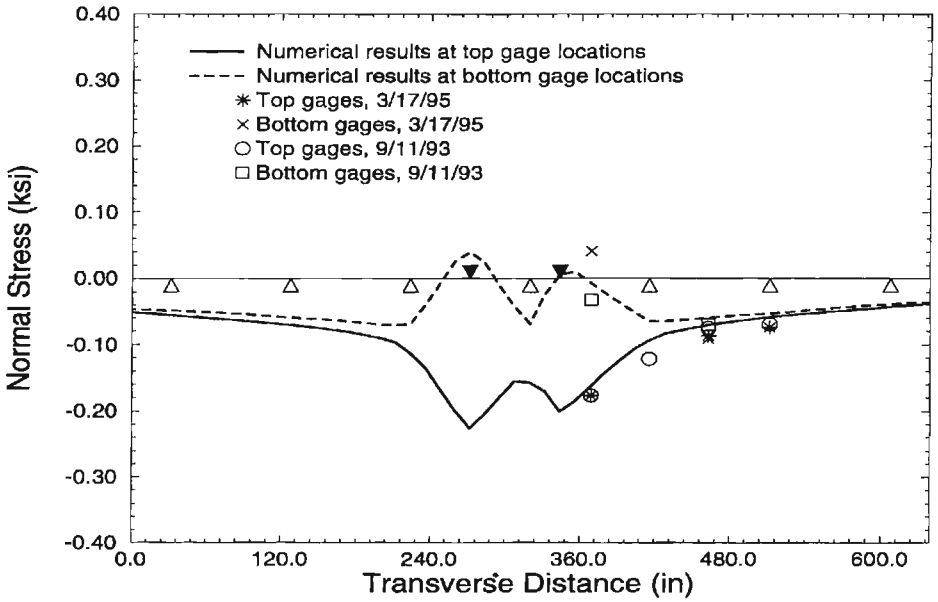

Figure C.6: Normal Stress in Longitudinal Direction along Gage Line 2 (Case 2B2)

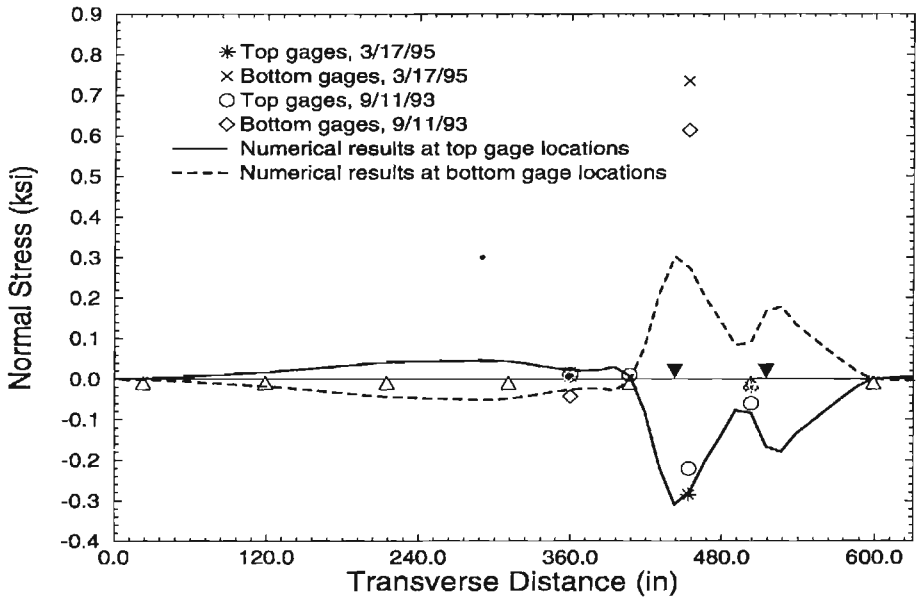

Figure C.7: Normal Stress in Transverse Direction along Gage Line 2 (Case 2C1)

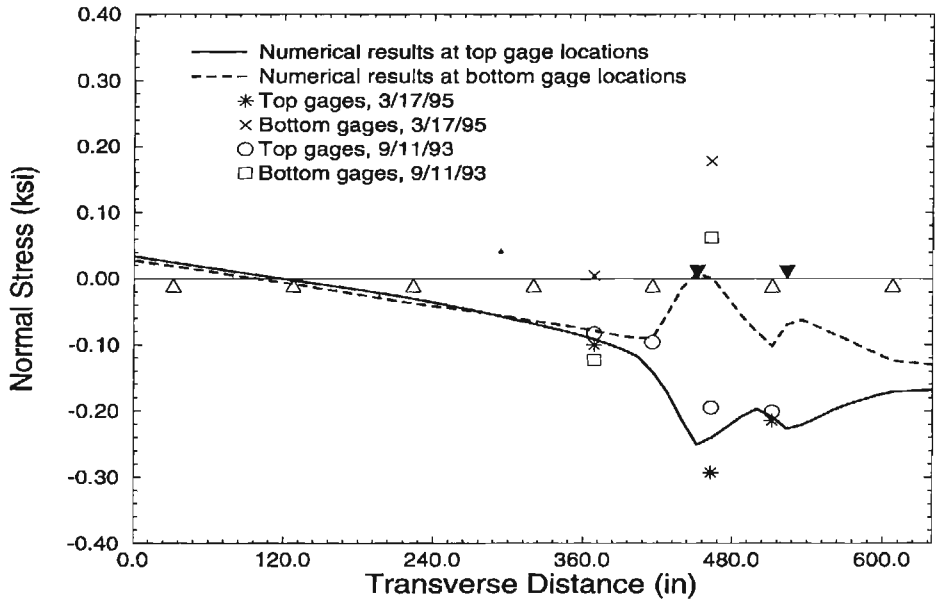

Figure C.8: Normal Stress in Longitudinal Direction along Gage Line 2 (Case 2C1)

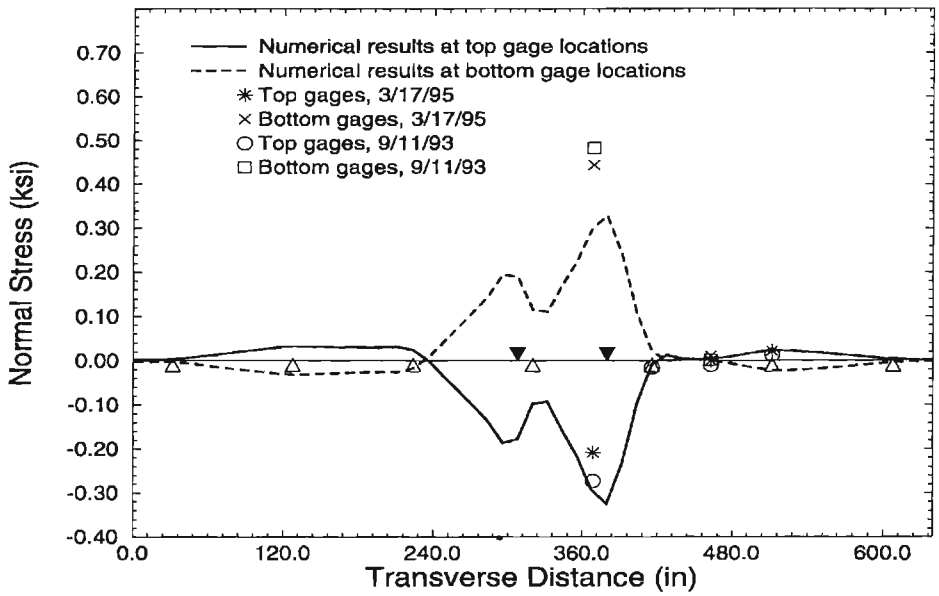

Figure C.9: Normal Stress in Transverse Direction along Gage Line 2 (Case 2C2)

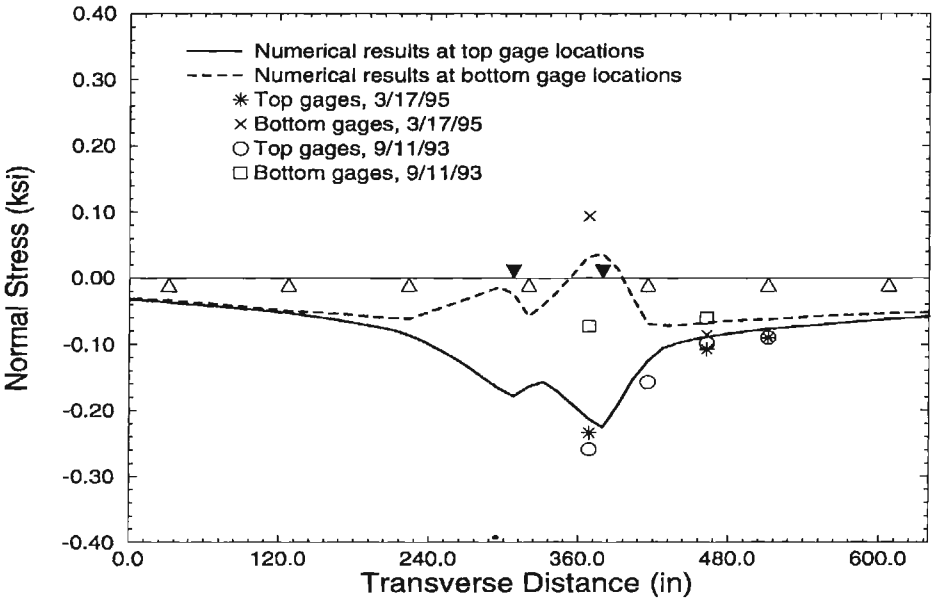

Figure C.10: Normal Stress in Longitudinal Direction along Gage Line 2 (Case 2C2)

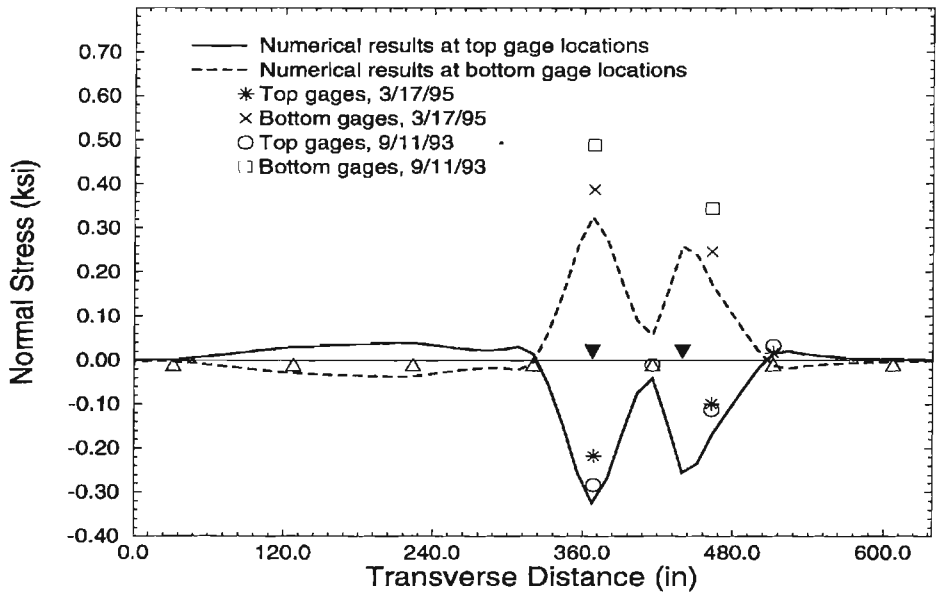

Figure C.11: Normal Stress in Transverse Direction along Gage Line 2 (Case 2D)

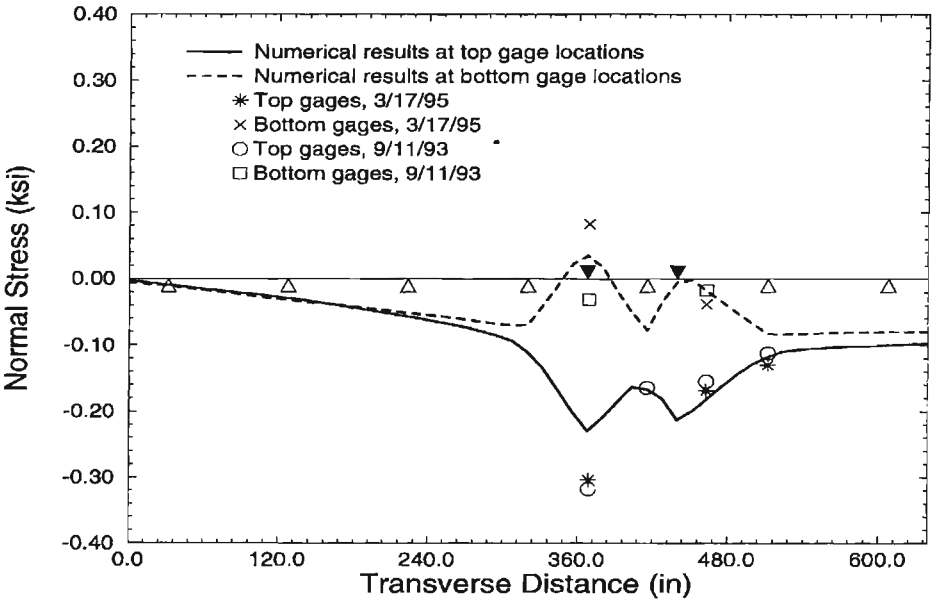

Figure C.12: Normal Stress in Longitudinal Direction along Gage Line 2 (Case 2D)

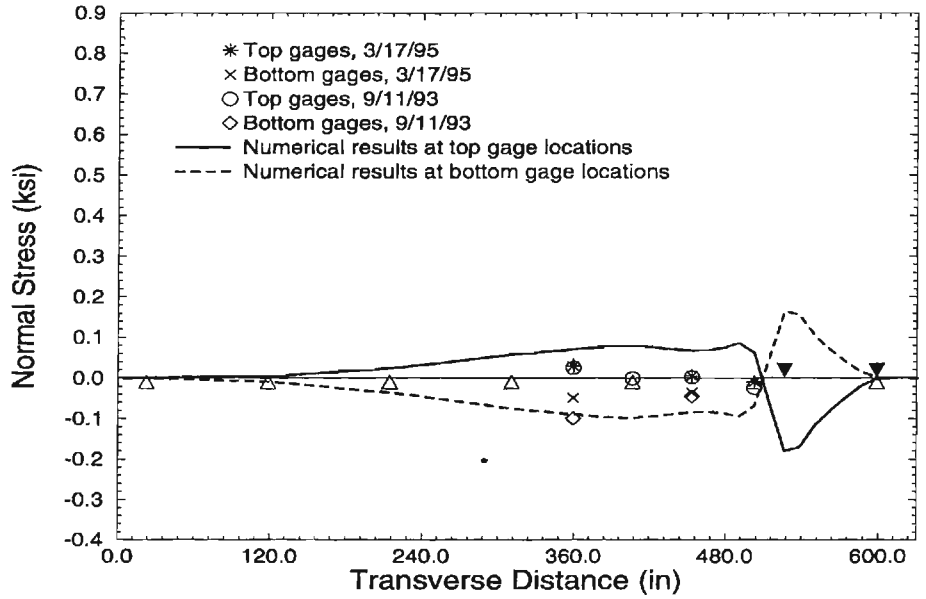

Figure C.13: Normal Stress in Transverse Direction along Gage Line 2 (Case 2E)

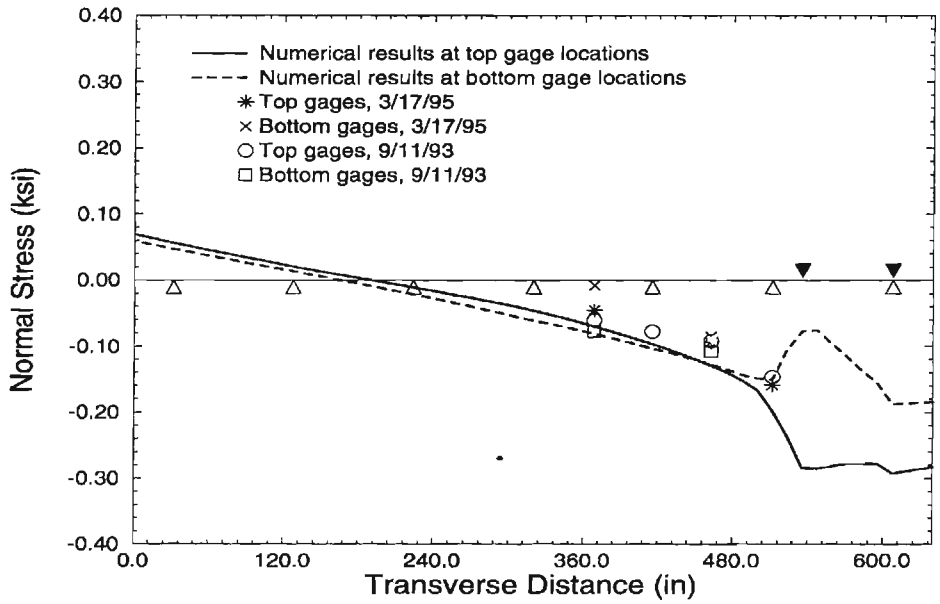

Figure C.14: Normal Stress in Longitudinal Direction along Gage Line 2 (Case 2E)